

**ULTRAFAST PHENOMENA IN GAAS/ALGAAS
MULTIPLE QUANTUM WELL WAVEGUIDE STRUCTURES
USING A NEAR INFRARED FEMTOSECOND LASER SYSTEM**

by

Paul Alexander Harten

A Dissertation Submitted to the Faculty of the
COMMITTEE ON OPTICAL SCIENCES (GRADUATE)

In Partial Fulfillment of the Requirements
For the Degree of

DOCTOR OF PHILOSOPHY

In the Graduate College of
THE UNIVERSITY OF ARIZONA

1 9 9 2

INFORMATION TO USERS

This manuscript has been reproduced from the microfilm master. UMI films the text directly from the original or copy submitted. Thus, some thesis and dissertation copies are in typewriter face, while others may be from any type of computer printer.

The quality of this reproduction is dependent upon the quality of the copy submitted. Broken or indistinct print, colored or poor quality illustrations and photographs, print bleedthrough, substandard margins, and improper alignment can adversely affect reproduction.

In the unlikely event that the author did not send UMI a complete manuscript and there are missing pages, these will be noted. Also, if unauthorized copyright material had to be removed, a note will indicate the deletion.

Oversize materials (e.g., maps, drawings, charts) are reproduced by sectioning the original, beginning at the upper left-hand corner and continuing from left to right in equal sections with small overlaps. Each original is also photographed in one exposure and is included in reduced form at the back of the book.

Photographs included in the original manuscript have been reproduced xerographically in this copy. Higher quality 6" x 9" black and white photographic prints are available for any photographs or illustrations appearing in this copy for an additional charge. Contact UMI directly to order.



University Microfilms International
A Bell & Howell Information Company
300 North Zeeb Road, Ann Arbor, MI 48106-1346 USA
313/761-4700 800/521-0600

Order Number 9303297

**Ultrafast phenomena in GaAs/AlGaAs multiple quantum well
waveguide structures using a near infrared femtosecond laser
system**

Harten, Paul Alexander, Ph.D.

The University of Arizona, 1992

U·M·I
300 N. Zeeb Rd.
Ann Arbor, MI 48106

**ULTRAFAST PHENOMENA IN GAAS/ALGAAS
MULTIPLE QUANTUM WELL WAVEGUIDE STRUCTURES
USING A NEAR INFRARED FEMTOSECOND LASER SYSTEM**

by

Paul Alexander Harten

A Dissertation Submitted to the Faculty of the
COMMITTEE ON OPTICAL SCIENCES (GRADUATE)

In Partial Fulfillment of the Requirements
For the Degree of

DOCTOR OF PHILOSOPHY

In the Graduate College of
THE UNIVERSITY OF ARIZONA

1 9 9 2

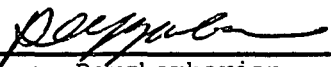
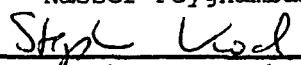
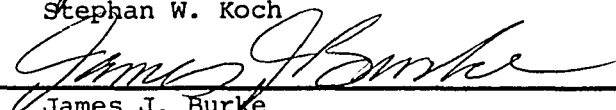
THE UNIVERSITY OF ARIZONA
GRADUATE COLLEGE

2

As members of the Final Examination Committee, we certify that we have
read the dissertation prepared by Paul Alexander Harten


entitled Ultrafast Phenomena in GaAs/AlGaAs Multiple Quantum
Well Waveguide Structures Using a Near Infrared Femto-
second Laser System

and recommend that it be accepted as fulfilling the dissertation
requirement for the Degree of Doctor of Philosophy

<u></u> Nasser Peyghambarian	<u>8/19/1992</u> Date
<u></u> Stephan W. Koch	<u>8/19/1992</u> Date
<u></u> James J. Burke	<u>8/19/1992</u> Date
<u></u>	<u></u> Date
<u></u>	<u></u> Date

Final approval and acceptance of this dissertation is contingent upon
the candidate's submission of the final copy of the dissertation to the
Graduate College.

I hereby certify that I have read this dissertation prepared under my
direction and recommend that it be accepted as fulfilling the dissertation
requirement.

<u></u> Dissertation Director Nasser Peyghambarian	<u>8/19/1992</u> Date
--	--------------------------

STATEMENT BY AUTHOR

This dissertation has been submitted in partial fulfillment of requirements for an advanced degree at The University of Arizona and is deposited in the University Library to be made available to borrowers under rules of the Library.

Brief quotations from this dissertation are allowable without special permission, provided that accurate acknowledgment of source is made. Requests for permission for extended quotation from or reproduction of this manuscript in whole or in part may be granted by the head of the major department or the Dean of the Graduate College when in his or her judgment the proposed use of the material is in the interests of scholarship. In all other instances, however, permission must be obtained from the author.

SIGNED: Paul A. Herten

Acknowledgements

"Wisdom is supreme; therefore get wisdom. Though it cost all you have, get understanding." (Proverbs, 4:7)

Without the supportive suggestions, constructive criticism, and help in the experimental and theoretical work from Rolf Binder, François Brown de Colstoun, Chi-Li Chuang, Brian D. Fluegel, Hyatt M. Gibbs, Ruxiang Jin, Galina Khitrova, Andreas Knorr, Stephan W. Koch, Sang-Goo Lee, Brian P. McGinnis, Kenith E. Meissner, Jason P. Sokoloff, and Ewan M. Wright this dissertation would not have been possible. Nasser Peyghambarian deserves special recognition for his guidance and support as a thesis director. I am indebted to Martin D. Dawson and Tibor Juhasz for valuable assistance in the construction of the near-infrared femtosecond laser system. Thanks to James J. Burke for correcting grammar and style of this dissertation. I would like to thank all of the Optical Sciences faculty, staff, and students, particularly the not explicitly mentioned members of Dr. Peyghambarian's group, for making the Ph.D. program an enjoyable experience. Fellowships by the Fulbright-Commission, the SPIE, and IBM are acknowledged.

This work would not have been finished without the support from my wife, Birgit Susanne, and the generosity of my parents in law.

To my parents

Table of Contents

	Page
List of Illustrations	8
Abstract	10

CHAPTER 1: NEAR INFRARED FEMTOSECOND LASER FACILITY

1.1. Introduction	14
1.2. Hybridly mode-locked femtosecond dye laser	15
1.3. Regenerative Nd:YAG pumped dye amplifier	18
1.4. Data acquisition system	23

CHAPTER 2: NOISE PROPERTIES OF THE DYE OSCILLATOR

2.1. Introduction	25
2.2. Theoretical concept	27
2.3. Noise power spectral measurements	31
2.4. Conclusion	40

CHAPTER 3: NONLINEAR DIRECTIONAL COUPLER

3.1.	Introduction	43
3.2.	The directional coupler device	45
3.3.	Experimental setup	48
3.4.	Observation of femtosecond all-optical switching	50
3.5.	Adiabatic following and optical Stark effect in semiconductor	55
3.6.	Conclusion	59

CHAPTER 4: SINGLE WAVEGUIDE COHERENT PULSE PROPAGATION

4.1.	Introduction	61
4.2.	Experimental setup	62
4.3.	Experimental observation of coherent pulse breakup	66
4.4.	Propagation-induced escape from adiabatic following	70
4.5.	Conclusion	82

CHAPTER 5: DIRECTIONAL COUPLER COHERENT PULSE PROPAGATION AND FUTURE EXPERIMENTS

5.1.	Preliminary coherent pulse propagation results in directional couplers	84
5.2.	Suggestions for Future Experiments	88

	7
Appendix: List of Publications	90
References	92

List of Illustrations

Figure		Page
1	Schematic of laser facility	15
2	Hybridly mode-locked dye laser cavity	16
3	Background free intensity autocorrelations and laser spectra of the dye oscillator for two slightly different cavity lengths	17
4	Regenerative Nd:YAG amplifier cavity	18
5	Pulse energy distribution of the frequency doubled regenerative Nd:YAG amplifier output	20
6	Schematic of dye amplifier	21
7	Pulse energy distribution of dye laser pulses following the first amplification stage and the saturable absorber	22
8	Data acquisition related physical connections between laboratory instruments . . .	23
9	Noise power spectra of the mode-locker synch out signal and the $\lambda = 532$ nm intensity of the Nd:YAG pump laser	32
10	Square dependence of the pump laser jitter noise data to the order number	34
11	Noise power spectra of the dye laser intensity at $\Delta L = -0.7 \mu\text{m}$	35
12	Noise power spectra of the dye laser intensity at $\Delta L = 0$	35
13	Lower resolution larger frequency span versions of Figures 12(a) and 11(a)	36
14	Intermediate frequency span versions of Figures 12(a) and 11(a)	37
15	Sample time interval of modelled random amplitude fluctuation function $A(t)$, autocorrelation $G_A(t)$ of $A(t)$, and logarithm of the normalized power spectrum $P_A(t)$ of $A(t)$	39
16	Noise power spectra of dye laser second harmonic intensity	41
17	Cross section of nonlinear directional coupler design	48
18	Configuration of nonlinear directional coupler all-optical switching experiment . .	49

19	Transverse transmitted probe beam profiles as a function of time delay. The inset schematically shows how the light is inserted into and propagates through the device with and without nonlinear coupling	51
20	Relative probe transmission as a function of pump intensity for both coupler channels	52
21	Total probe beam transmission versus time delay	53
22	Relative probe beam transmission as a function of time delay and lack of recovery as a function of pump intensity for both coupler channels	54
23	Calculated dynamic behavior of exciton absorption and carrier density under the optical Stark effect	59
24	Cross-correlator setup	63
25	Cross section of single waveguide design	64
26	Input pulse characteristics for the single waveguide pulse propagation experiment dye laser pulse train	65
27	Measured transmitted pulse shapes and spectra of a 0.37 mm long waveguide . . .	67
28	Picosecond pulse cross-correlations and spectra without waveguide and of a 0.41 mm long waveguide	68
29	Measured transmitted pulse shapes and spectra of a 1.5 mm long waveguide . . .	69
30	Theoretical pulse shape and spectral results for the 0.37 mm long waveguide . . .	74
31	Theoretical pulse shapes and spectral results for the 1.5 mm long waveguide . . .	76
32	Calculated pulse intensity and total carrier density profiles as a function of propagation distance	79
33	Calculated frequency chirp at $\xi = 120 \mu\text{m}$ propagation distance and temporal profiles of the carrier density at $\xi = 120 \mu\text{m}$ resulting from solving the semiconductor Bloch equations with the exact numerical phase solution, a first order fit, and a second order fit	82
34	Time-integrated outputs of the directional coupler channels for single input pulses with peak intensities below and above the switching point	85
35	Cross-correlations of the 0.88 mm directional coupler outputs with the input intensities of Figure 34	86
36	Spectral output intensities of the 0.88 mm directional coupler channels	87

Abstract

A near infrared hybridly mode-locked dye laser system consisting of a femtosecond oscillator and a high repetition rate dye amplifier was designed and built. This system was then applied to the study of room temperature below-bandgap femtosecond switching and coherent pulse propagation in GaAs/GaAlAs multiple quantum well waveguides.

The noise properties of the oscillator output were studied using radio frequency spectrum analysis techniques. Two distinct modes of operation were identified: The first is characterized by the shortest pulse duration and its real-time autocorrelation signal appears more strongly modulated. The second mode of operation, which exhibits a slightly longer pulse duration and a smoother real-time autocorrelation signal, is obtained for a relative cavity length detuning of $\Delta L = -0.7 \mu\text{m}$. Unexpectedly, the second mode features larger pulse duration fluctuations than the first mode and self-pulsing, while the pulse repetition timing and pulse energy fluctuations were found to be similar in both cases, making the first mode preferable for use in time-resolved experiments.

Femtosecond all-optical switching under off-resonance room temperature excitation was demonstrated in a passive GaAs/AlGaAs multiple quantum well directional coupler for the first time. The required phase mismatch originates from an ultrafast refractive index change caused by the optical Stark effect. The main obstacle regarding practical device applications is its low transmission (less than 10 %). The use of electrically pumped semiconductor waveguides that provide gain promises to remove this disadvantage.

Below-resonance, coherent pulse breakup in a room temperature semiconductor waveguide was observed for the first time. Numerical simulations of the coupled semiconductor Maxwell-Bloch equations show that the light-matter interaction can induce enough chirp through self-phase modulation during propagation in order to violate the initial adiabatic following regime and cause pulse breakup. This coherent effect is distinctly different from self-induced transparency, because it does not involve Rabi-oscillations at the start of propagation, from temporal solitons, because it does not require group velocity dispersion, and from self-steepening. However, it should be ubiquitous under off-resonance pulse propagation with a pulse duration less than the polarization dephasing time.

Introductory Remarks

Optical devices are very attractive for communication links due to three advantageous features: Wide bandwidth, high signal propagation speed, and insensitivity to electrical interference. A very good, if not the best, example for a technology that exploits these advantages is the optical fiber combined with semiconductor lasers and optical amplifiers. These communication systems, which have only recently reached maturity, have already replaced many electronic long-distance transmission lines, greatly improving signal handling capabilities.

Researchers are now trying to develop integrated optical devices that are able to extend the domain of optical communications down to the circuit board and microchip level. The materials for such optical integrated circuits should ideally have low losses *and* large optical nonlinearities, permitting easy fabrication of optically bistable devices.

The optical response in the energy range close to the bandedge of bulk semiconductors and semiconductor microstructures has been known to give rise to a variety of nonlinear optical phenomena. The recent progress in semiconductor fabrication techniques, which is driven by a rapid growth in the computer industry, has made it possible to produce high purity microstructures of these materials with atomic monolayer size control. These two, one, or even zero dimensional structures promise to provide enhanced nonlinear response compared to bulk material [see Peyghambarian and Koch, 1991, and references therein].

In waveguide devices, similar to the glass fiber, the nonlinear optical properties can be utilized very efficiently due to the confinement of high intensity light beams in a small guiding

volume throughout long propagation distances. If femtosecond light pulses are employed, not only are high peak intensities available for the generation of a nonlinear response at low average power, but the dynamics of the light-matter interaction may be studied in both time and frequency domains.

After summarizing the motivation for this work a brief description of the content will conclude the introduction. The dissertation can be divided into two main sections. The first section, which comprises chapters 1 and 2, is dedicated to the description of the laser system that has been built to study the properties of GaAs/AlGaAs multiple quantum wells (MQWs) and MQW waveguide structures. The second section, which encompasses chapters 3 and 4, depicts two significant experiments conducted with this laser system.

CHAPTER 1

NEAR INFRARED FEMTOSECOND LASER FACILITY

1.1. Introduction

Before the arrival of the self-mode-locked Ti:sapphire technology [Spence et al., 1991] only the hybridly mode-locked dye laser was available for femtosecond pulse generation with wavelengths beyond 850 nm [Smith et al., 1984; Dobler et al., 1986; Dawson et al., 1987]. The dye oscillator used throughout this work is designed following Dawson et al. [Dawson et al., 1986]. Its mode-locked output wavelength range between 865 nm and 875 nm is close to the bandedge of GaAs at room temperature, making it suitable for femtosecond spectroscopy of GaAs and related materials, in particular the new quasi-two-dimensional quantum well or superlattice structures.

Figure 1 gives an outline of the main components of the laser facility. A continuous-wave, mode-locked, frequency doubled Nd:YAG laser serves as the pump source for the near-infrared hybridly mode-locked dye oscillator. The mode-locker driver unit of this Nd:YAG laser also serves as synchronization reference for the complete facility and part of its fundamental frequency output feeds the regenerative Nd:YAG amplifier. The output of the dye laser is amplified in dye flow cells that are pumped by the frequency doubled regenerative amplifier emission. A continuously scanning background-free autocorrelator provides real-time information about the dye laser pulse shape [Diels et al., 1985]. The box marked "experiment" in Figure 1 represents different experimental setups that will be described in detail in the chapters of this dissertation.

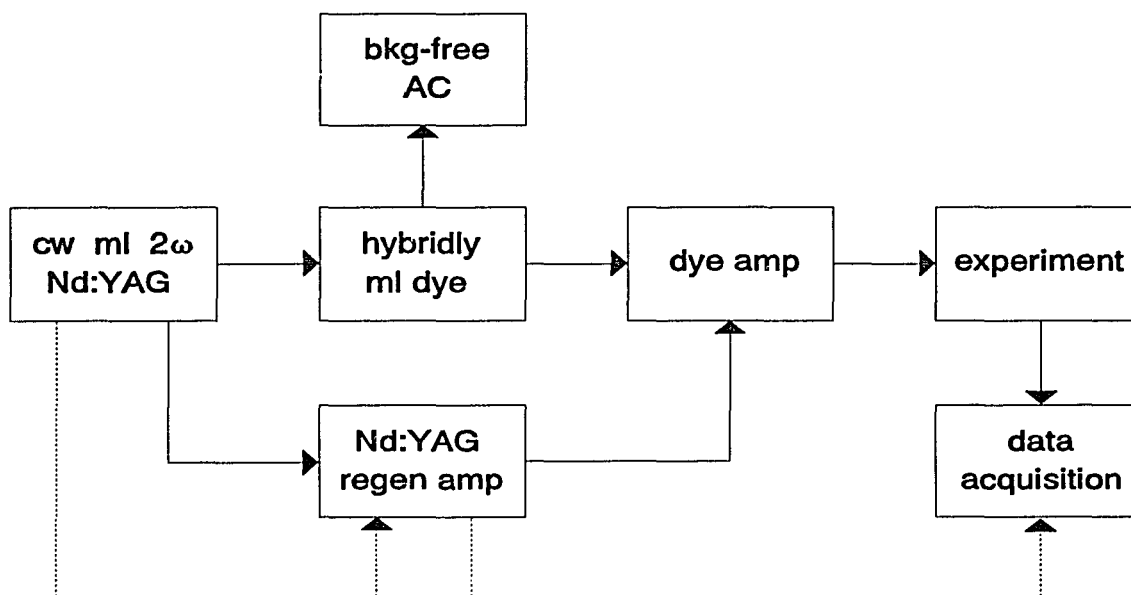


Figure 1. Schematic of laser facility using the following abbreviations: Cw ml 2 ω Nd:YAG...frequency doubled cw mode-locked Nd:YAG laser, hybridly ml dye...hybridly mode-locked dye laser, bkg-free AC...background-free autocorrelator, dye amp...dye amplifier, Nd:YAG regen amp...regenerative Nd:YAG amplifier. Solid lines indicate optical connections, dashed lines indicate electrical connections.

1.2. Hybridly mode-locked femtosecond dye laser

Figure 2 schematically displays the dye laser cavity. Quartz Brewster prisms, in double pass operation, provide for group velocity compensation and effectively compress the pulse as it circulates inside the cavity [Fork et al., 1984]. The $T = 10\%$ output coupler is mounted on a piezoelectrically adjustable translation stage for cavity length fine tuning with sub-micron resolution. The gain dye is pumped with 650 mW average power by the frequency doubled

Nd:YAG laser and the output pulse train consists of ≈ 100 fs full-width-at-half-maximum (FWHM) pulses of about 0.3 nJ pulse energy at 82 MHz repetition rate. Higher pump power causes double pulsing and is therefore not desirable.

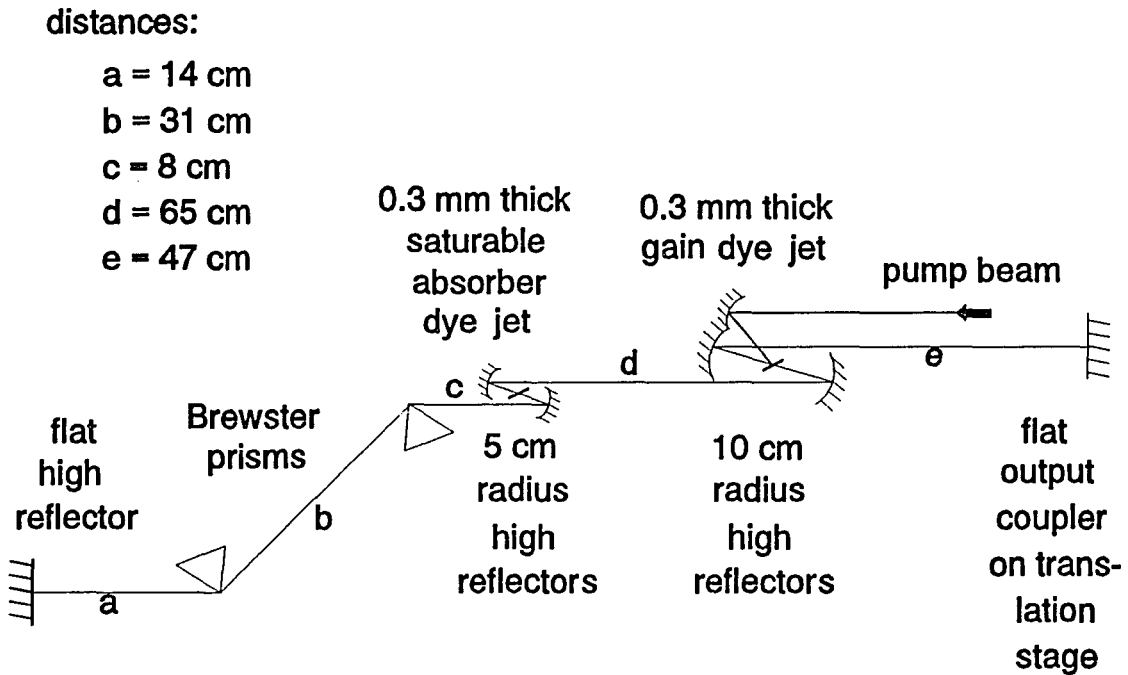


Figure 2. Hybridly mode-locked dye laser cavity.

The output of the dye oscillator exhibits two different modes of operation which are distinguished by slightly different cavity lengths, pulse and spectral widths, as well as noise characteristics: The first is characterized by the shortest pulse duration and its real-time autocorrelation signal (Figure 3 (a)) appears more strongly modulated. The second mode of operation, which exhibits a slightly longer pulse duration and a smoother real-time autocorrelation

signal (Figure 3 (b)), is obtained for a relative cavity length detuning of about $\Delta L = -0.7 \mu\text{m}$. The differences between these two modes are further investigated in chapter 2, exploiting their noise characteristics. The small pulse duration increase from Figure 3 (a) to (b) is offset by a spectral width decrease, leaving the time-bandwidth product constant at $\Delta\nu \cdot \Delta t_p = 0.2$. This shows that the pulses are approximately transform limited in both cases, i. e. the Fourier transform of the temporal electric field envelope equals the spectral distribution of the electric field. It further suggests an asymmetric pulse shape. While all common symmetric pulse shapes have a time-bandwidth product exceeding 0.3, the introduction of asymmetry changes this number to less than 0.3 [Diels et al., 1985].

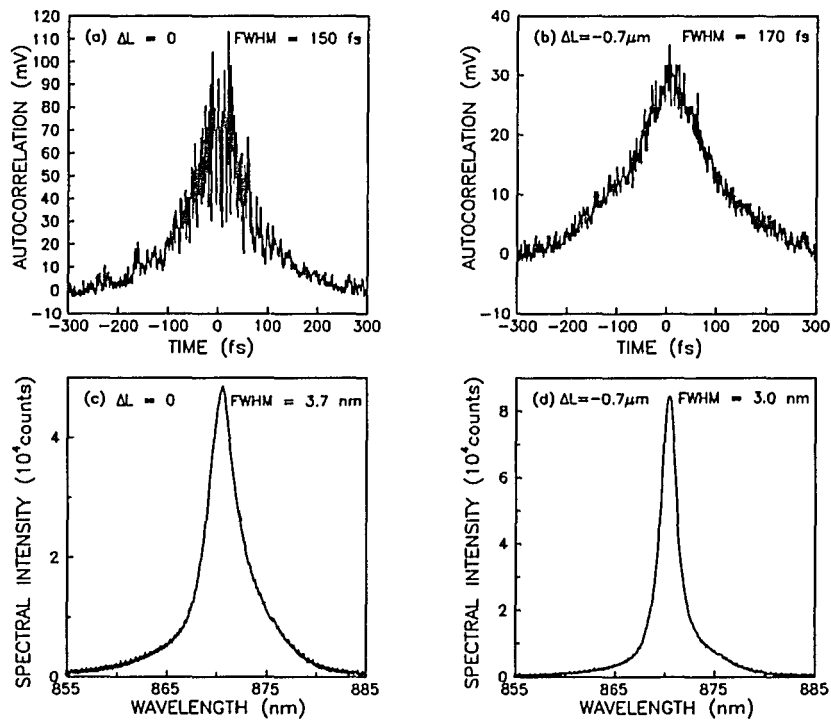


Figure 3. Background free intensity autocorrelations and laser spectra of the dye oscillator for two slightly different cavity lengths very close to the pump laser length.

1.3. Regenerative Nd:YAG pumped dye amplifier

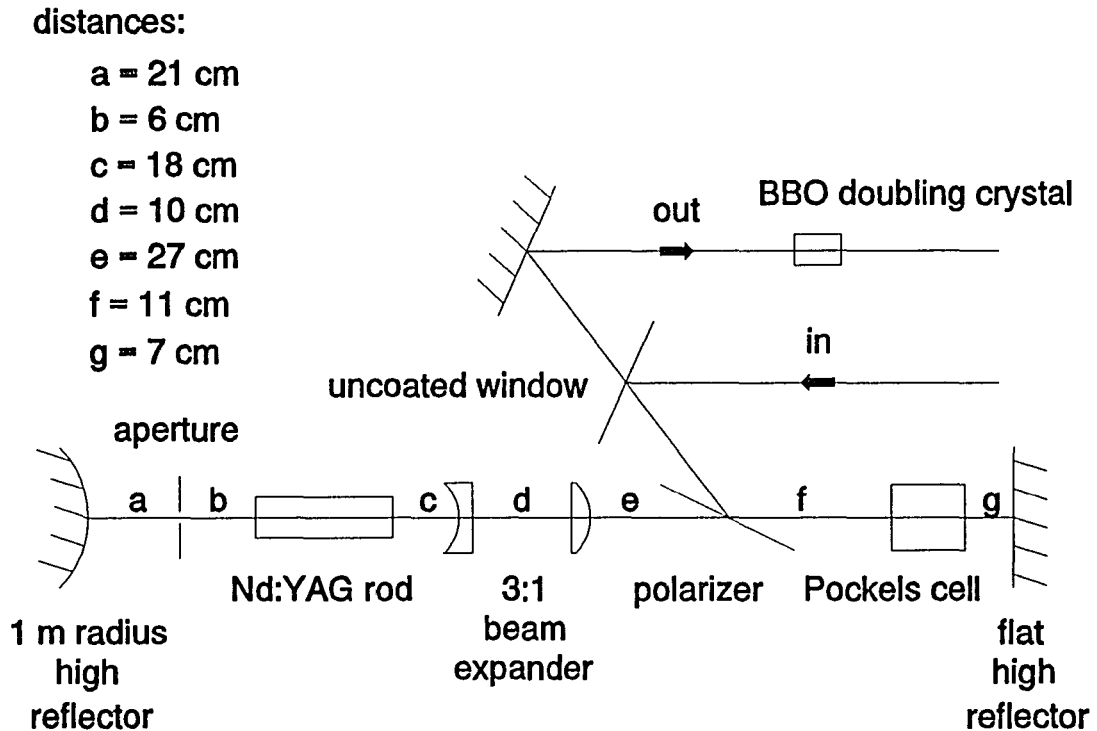


Figure 4. Regenerative Nd:YAG amplifier cavity. Input (seed beam): 100 ps FWHM pulses at 82 MHz, 200 mW average power, from cw mode-locked Nd:YAG laser; output: 100 ps FWHM pulses at 1 kHz, 1 W average power.

Amplification of the dye oscillator output makes it possible to reach the threshold intensities for most nonlinear optical effects including generation of broad new frequency bands centered around the laser frequency, known as white light or continuum generation. The latter is crucial for ultrafast time-resolved spectroscopy, because it allows for monitoring spectral changes in materials of interest over a large bandwidth on a timescale of 100 fs or less.

Continuum generation requires pulse energies on the order of $1 \mu\text{J}$, if visible light pulses are focussed into an Ethylene Glycol jet. Thresholds have been measured to be three to four times higher in the near infrared spectral region [Knox, 1987; Olbright and Hadley, 1988]. Various schemes have been successfully used to reach these pulse energies [Knox, 1988]. We chose a regenerative Nd:YAG based amplification scheme [Juhasz et al., 1988], because it avoids the extreme maintenance problems associated with copper vapor lasers while it still allows data acquisition at a repetition rate of 1 kHz.

Figure 4 shows the regenerative Nd:YAG amplifier cavity. Part of the fundamental frequency output of the cw mode-locked Nd:YAG laser serves as seed beam for the regenerative amplifier. In the unactivated (no voltage applied) state the Pockels cell is oriented for quarterwave retardation. This causes each seed pulse entering the regenerative amplifier cavity to be ejected after one round trip. A single seed pulse can be picked out of the pulse train and trapped inside the regenerative amplifier when the Pockels cell is switched (risetime $< 5 \text{ ns}$) up to quarterwave voltage while the pulse is to the left of the polarizer in Figure 4. At this voltage level the Pockels cell acts as a halfwave plate. After the trapped pulse has depleted the available gain, which takes several tens of roundtrips in arc lamp pumped Nd:YAG gain media, it is ejected. This is achieved by switching the Pockels cell up to halfwave voltage which reduces its retardation to the initial quarterwave value. The output pulse is frequency doubled (about 50 % doubling efficiency without focussing the incident beam) in a second-harmonic generating crystal (BBO). A dichroic beamsplitter separates the second harmonic from the fundamental frequency and sends the $\lambda = 532 \text{ nm}$ beam into an adjustable delay line which creates the necessary temporal overlap between the regenerative amplifier output and the dye oscillator pulse train.

Figure 5 shows the pulse energy distribution of the regenerative amplifier's $\lambda = 532 \text{ nm}$

output. The distribution width is $\Delta E = 0.17 E_{\text{peak}}$ (FWHM), where $E_{\text{peak}} = 0.5 \text{ mJ}$ is the pulse energy at the peak of the distribution. These pulses are split by an 80 % transmitting and 20 % reflecting beamsplitter into two parts to pump two dye amplifier stages as presented in Figure 6. The less intense beam pumps the first (preamplifier) stage, the other beam pumps the second amplifier stage. The regenerative amplifier beams and the dye laser beams are both focussed by the same lenses into each dye flow cell.

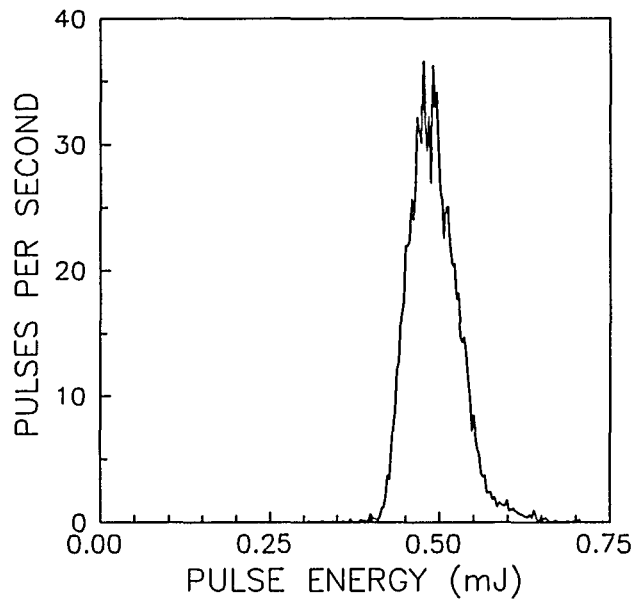


Figure 5. Pulse energy distribution of the $\lambda = 532 \text{ nm}$ regenerative Nd:YAG amplifier output.

The transmitted (about 10 %) green pump light is blocked by irises behind each dye cell. After the first amplifier stage the unamplified dye laser pulses are eliminated by a thin piece of bulk GaAs which operates as a saturable absorber [Knox, 1987]. The leading edge of the amplified

pulse saturates the absorption and allows the rest of the pulse to pass through almost unattenuated. After the second amplifier stage, part of the amplified dye laser pulse can be split off as a pump pulse that excites the material under study in pump - probe experiments. The bigger portion of the amplified pulse is fed into a single mode optical fiber to generate a frequency continuum. Group velocity dispersion in the fiber causes also temporal spreading, which is compensated by a prism pulse compressor as shown in Figure 6 [Bor and Rácz, 1985; Kafka and Baer, 1987].

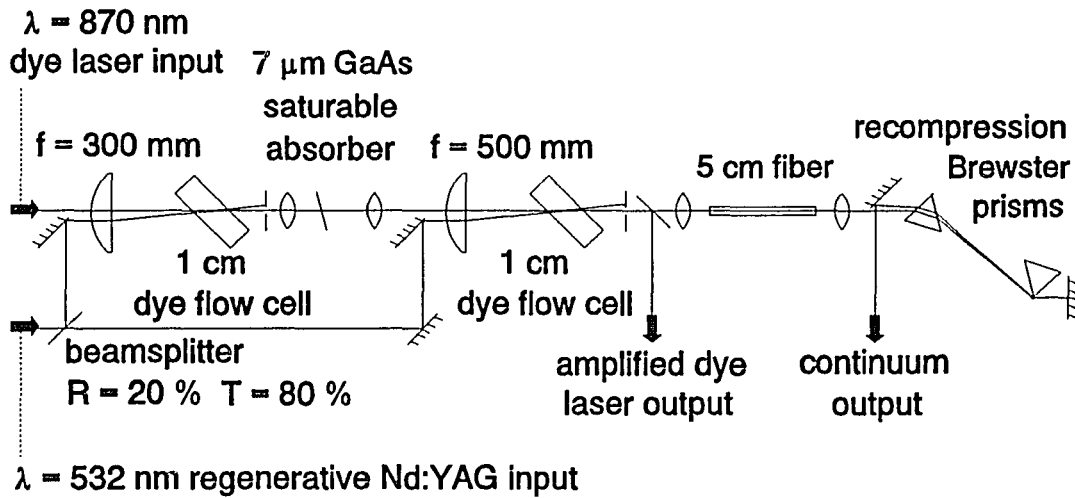


Figure 6. Schematic of dye amplifier.

Figure 7 shows a histogram of dye laser pulse energies after the first amplifier stage and the saturable absorber. This distribution has a width of $\Delta E = 0.4 E_{\text{peak}}$ (FWHM), where E_{peak}

= 7.5 nJ, which is more than twice as large as the width of the regenerative amplifier histogram, indicating significant pulse energy noise in the dye oscillator. This noise is described in detail in the next chapter.

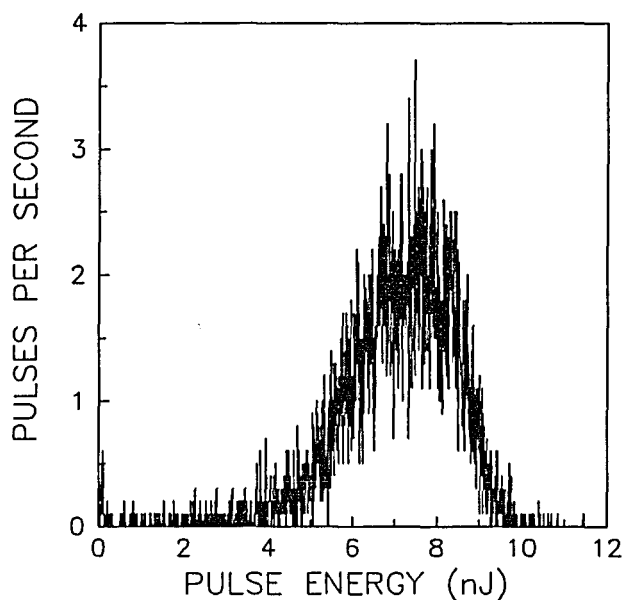


Figure 7. Pulse energy distribution of dye laser pulses following the first amplification stage and the saturable absorber.

The changes in dye laser spectrum and autocorrelation introduced by the amplification process are small. This is due to the large gain bandwidth of the amplifier dye (LDS 867), which provides spectrally uniform gain across the laser bandwidth. It also indicates that gain depletion is avoided. Temporal pulse broadening due to group velocity dispersion in the amplifier is offset by adjusting the intracavity prisms in the dye oscillator for the appropriate amount of chirp, in order to obtain the shortest autocorrelation width after the amplifier.

1.4. Data acquisition system

Time averaged and continuous wave spectral measurements are performed with the combination of a Spex 0.34 m spectrometer and an EG&G OMA III silicon photodiode array. Since the OMA data are MS-DOS compatible, they can be immediately processed on the DECstation 333c personal computer, which controls most of the remaining laboratory data instruments. The computer contains a digital-to-analog (D/A) and analog-to-digital (A/D) conversion card, a frame-grabber for video camera image recording, and a GPIB interface. Figure 8 illustrates the physical connections of the laboratory data acquisition system.

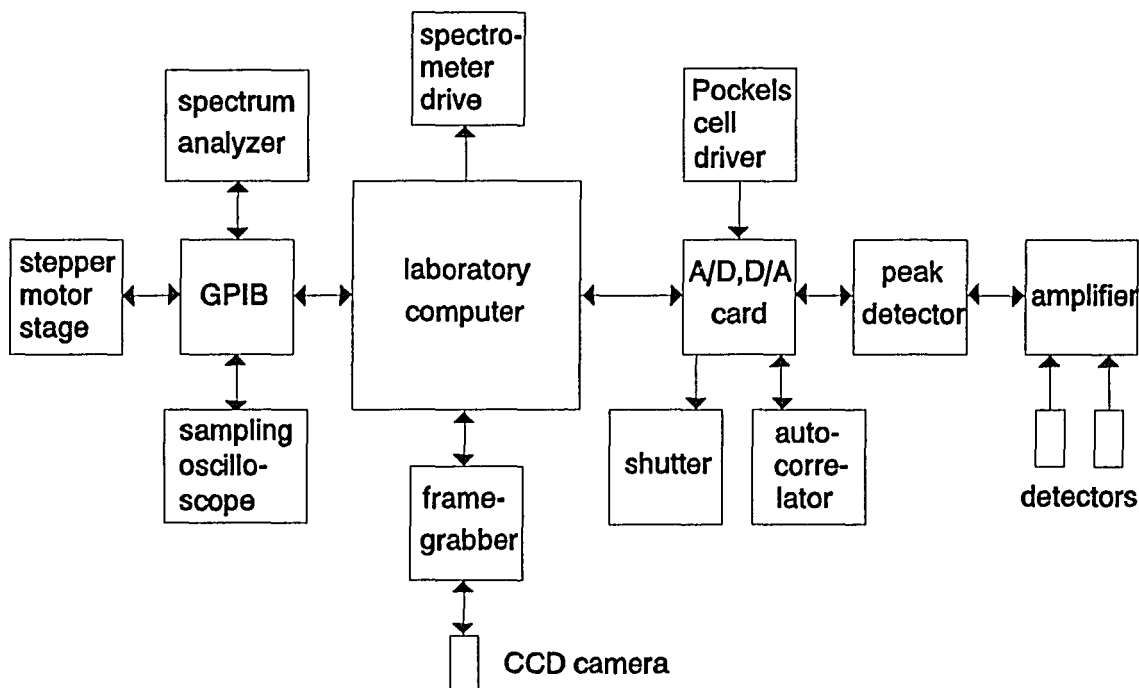


Figure 8. Data acquisition related physical connections between laboratory instruments.

The most frequently used data acquisition mode involves two detectors, usually one photomultiplier tube for the signal of interest and one reference photodiode for the incident pulse energy. The signals are converted from current to voltage by amplifiers that feed peak detectors, which are read out by the computer controlled A/D board. Synchronization of the data readout, the peak detector reset, and the shutter open and close cycles (for background subtraction) with the amplified dye laser pulse train is supplied by the Pockels cell driver unit.

CHAPTER 2

NOISE PROPERTIES OF THE DYE OSCILLATOR

2.1. Introduction

Hybridly mode-locked dye lasers have been used extensively in ultrafast spectroscopy experiments. This is mainly due to the larger number of gain and saturable absorber dye combinations available as compared to passively mode-locked systems and the ease of synchronization with amplifiers and other lasers that are synchronously pumped in parallel. Hybrid mode-locking introduces a saturable absorber assembly into a synchronously pumped laser cavity, combining passive and active mode-locking mechanisms. The saturable absorber provides an additional pulse shortening mechanism by cutting off the leading edge of the pulse. The widespread use and the complexity of these systems have led to a number of different theoretical and experimental approaches to characterize them [Ausschnitt et al., 1979; Casperson et al., 1983; MacFarlane et al., 1990; Petrov et al., 1989].

One of the characteristics of this type of mode-locking is its extreme sensitivity to cavity length mismatch between the pump laser and the dye laser. A previous study has established the general dependence of pulse width and spectrum on the cavity detuning [Dawson, 1988]. We have verified this general behavior for our laser. In addition, we observe in our experimental set up two cavity length positions close to the optimum length that yield transform limited pulses with durations of ≈ 100 fs, while exhibiting quite different scanning intensity autocorrelations. These small cavity length detuning regimes are of particular interest, because almost all hybridly

mode-locked dye laser applications demand transform limited and stable femtosecond pulse trains. The difference in operating characteristics between these two modes of operation is the object of this study.

Autocorrelation measurements are generally insufficient for the characterization of the laser output. In particular, they are not sufficient to uniquely determine a stable femtosecond pulse train. For this reason the random fluctuations of pulse energy and pulse duration are investigated employing the technique of radio frequency spectrum analysis [von der Linde, 1986; Harten et al., 1992]. This technique is based on recording the power spectrum of the laser intensity with the help of a fast photodiode and an electronic spectrum analyzer. The different random contributions to the laser noise are identified by their characteristic spectral appearances. Studies on similar laser systems using this technique have provided valuable insight into the noise properties of those systems [MacFarlane et al., 1988; von der Linde, 1986; Kluge et al., 1988]. MacFarlane et al. investigated a hybridly mode-locked dye laser experimentally and theoretically in terms of time of occurrence of the output pulses. They found that the time of occurrence stabilizes for shorter pump pulses of higher power, reducing the repetition time jitter of their laser system. Von der Linde's study presented the theoretical foundations for radio frequency spectrum analysis of continuous mode-locked lasers. Applying this formalism he found that the timing jitter of the pump laser is transferred directly to the dye laser in a synchronously mode-locked system. The relative timing jitter between the pump laser and the dye laser can therefore be very small. Kluge et al. found this to be true also for a hybridly mode-locked dye laser that combined saturable absorber and gain dye in a single mixed dye jet.

2.2. Theoretical concept

Following the treatment of von der Linde [von der Linde, 1986] the output intensity $F_0(t)$ of a perfectly mode-locked laser can be written

$$F_0(t) = \sum_n f(t+nT) , \quad (1)$$

where $f(t)$ is the temporal intensity profile of a single pulse, T is the repetition time of the pulses in the train, and the integer n runs from $-\infty$ to $+\infty$. The output intensity of an imperfectly mode-locked laser $F(t)$,

$$F(t) = \sum_n (1 + \delta f_n) f(t+nT + \delta T_n) , \quad (2)$$

is characterized by random intensity fluctuations δf_n and by random fluctuations in the repetition time δT_n which are considered to be small compared to $f(t)$ and T , respectively. With a Taylor expansion of $f(t+nT+\delta T_n)$ to first order in δT_n around $t+nT$,

$$f(t+nT+\delta T_n) = f(t+nT) + \frac{d}{dt} f(t+nT) \delta T_n , \quad (3)$$

and introducing two continuous random functions $A(t) = \delta f_n$ and $J(t) = \delta T_n/T$, Equation 2 can be recast into the form

$$F(t) = [1 + A(t)]F_0(t) + TJ(t)\frac{d}{dt}F_0(t) , \quad (4)$$

where $J(t)$ represents the timing jitter, and $A(t)$ represents the intensity fluctuations of the pulse train with time averages $\langle A(t) \rangle = \langle J(t) \rangle = 0$. This description is valid for random fluctuations that vary slowly compared to the pulse intensity $f(t)$. The quantity that can be measured with an electronic spectrum analyzer is the power spectrum $P_F(\omega)$ of the laser intensity. It is defined as the ensemble average over the square of the absolute value of its Fourier transform. In this case one obtains

$$P_F(\omega) = P_F^{env}(\omega) \sum_n [\delta(\omega_n) + P_A(\omega_n) + (2\pi n)^2 P_J(\omega_n)] , \quad (5)$$

with the envelope function

$$P_F^{env}(\omega) = (2\pi/T)^2 |g(\omega)|^2 , \quad (6)$$

where $g(\omega)$ denotes the Fourier transform of $f(t)$, $P_A(\omega)$ is the power spectrum of $A(t)$, $P_J(\omega)$ is the power spectrum of $J(t)$, and $\omega_n = \omega - 2\pi n/T$. Centered around each multiple of the repetition frequency one finds the same amplitude fluctuation power spectrum, $P_A(\omega)$, and, added to that, the timing jitter noise power spectrum $P_J(\omega)$ multiplied by the square of the order number n . For higher and higher order numbers the spectra will eventually decrease in magnitude due to the limited frequency range of the detection system. The bandwidth of the detection system used here is large enough to measure to at least $n = 18$. Therefore the amplitude noise can be obtained from the lowest order spectra while the jitter noise, which is recognized by its dependence on the order number, can be determined from the higher order spectra. The r.m.s. deviations of the pulse energy ΔE and the repetition time ΔT are related to the power spectra by [von der Linde, 1986]

$$(\Delta E/E)^2 = \int_{-\infty}^{+\infty} P_A(\omega) d\omega \quad (7)$$

and

$$(\Delta T/T)^2 = \int_{-\infty}^{+\infty} P_J(\omega) d\omega . \quad (8)$$

The integrals on the right hand sides of these equations are evaluated by integrating Equation 5 using several approximations. The first one relies on the assumption that $|g(\omega)|^2$ is not varying considerably between the $n = 1$ and $n = 18$ noise spectra. Then the envelope function $P_F^{env}(\omega)$ becomes a constant and can be pulled out of the integral. Each spectrum analyzer data point is already a result of an automatic integration over its resolution bandwidth Δf_{res} . Due to this fact one can relate the power spectrum peak value of the n th measured order, $p_{max,n}$, to the envelope function

$$P_F^{env}(\omega) = p_{max,n} \Delta f_{res} . \quad (9)$$

Equation 7 may be easily solved with the further assumption that for the $n = 1$ order the integral over the timing jitter term can be ignored, because it is much smaller than the integral over the amplitude noise. Then an integral S_1 over $P_F(\omega)$, encompassing the whole $n = 1$ noise band with the exception of a small region around ω_1 of the size $\pm \Delta f_{res}$, yields the desired right hand side of Equation 7 times the envelope function. In short

$$\int_{-\infty}^{+\infty} P_A(\omega) d\omega \approx \frac{S_1}{p_{max,1} \Delta f_{res}} . \quad (10)$$

One cannot neglect the timing jitter contribution in Equation 5 for high order numbers

n. In the experimental section 2.3. it is shown that the $n = 10$ component contains considerable timing noise contributions. In that case the timing jitter may be extracted by an additional similar integration, as described above for the amplitude fluctuations. This additional integral, S_{10} , covers the region around the $n = 10$ spectral peak in the same manner as before. Then

$$\int_{-\infty}^{+\infty} P_J(\omega) d\omega \cong \frac{1}{(20\pi)^2} \frac{S_{10} - S_1}{P_{\max,10} \Delta f_{res}} . \quad (11)$$

The integrations S_1 and S_{10} are numerically evaluated by summing the measured data points over the specified range.

Given the pulse energy fluctuations at both the fundamental (subscript "fund") and the second harmonic laser frequencies (subscript "sh"), and assuming a constant pulse shape, the r.m.s. pulse duration fluctuations, $\Delta t_p/t_p$, can be calculated [von der Linde, 1986]:

$$(\Delta t_p/t_p)^2 = (\Delta E/E)_{sh}^2 - 4(\Delta E/E)_{fund}^2 . \quad (12)$$

The special case of intensity fluctuations $A(t)$ that vary on the timescale of the pulse or faster with $\langle A(t) \rangle = 0$ and $\langle A^2(t) \rangle = 1$ is known as the noise burst model [Pike and Hercher, 1970]. In this case it is possible to derive an exact expression for the pulse energy fluctuations [von der Linde, 1986] as $\Delta E/E = (t_n/t_p)^{1/2}$, where t_n is the width of the random pulse substructure autocorrelation, and t_p is the width of the pulse envelope autocorrelation. It is straight forward to include a timing jitter term in the noise-burst model and then evaluate the measured noise power spectra as summarized above in Equations 7 and 8. We will show, however, that this model is not appropriate for noise analysis in our dye laser with small cavity

length detunings, because it leads to a too large amplitude fluctuation value.

2.3. Noise power spectral measurements

It is convenient to label the two distinctly different regimes of operation that were defined in chapter 1.2. by their cavity length mismatches as measured from some reference value. The optimum dye laser cavity length, which by this definition will be labelled as $\Delta L = 0$, is assumed to correspond to the cavity length which yields the shortest pulses as measured by their autocorrelation function. This cavity length does not, in general, correspond exactly to the pump laser cavity length, nor does it necessarily coincide with the dye laser cavity length that yields maximum second harmonic generation [Ausschnitt et al., 1979; Dawson et al., 1988]. The first mode of operation, which is characterized by larger peak second harmonic generation, shortest pulses, and a somewhat "noisier" autocorrelation (Figure 3 (a), page 16), will then be labeled $\Delta L = 0$. The second mode of operation, which yields slightly longer pulses and a smoother autocorrelation (Figure 3 (b)), will be referred to by $\Delta L = -0.7 \mu\text{m}$.

The sensitivity of the dye oscillator to extremely small cavity length mismatches implies, at least, that cavity length fluctuation induced noise is directly transferred from the pump laser to the dye laser. These fluctuations can be identified by comparing the pump laser noise with the dye laser noise. Figures 9 (b) and 9 (c) show power spectra of the frequency doubled Nd:YAG output centered at 82 MHz and 822 MHz, respectively. The 0 dB level corresponds to 10 dBm electrical power into the spectrum analyzer for all measured noise power spectra. Since the pump laser behavior is expected to be strongly dependent on the mode-locker, a power spectrum of the mode-locker "synch out" signal is also included as Figure 9 (a).

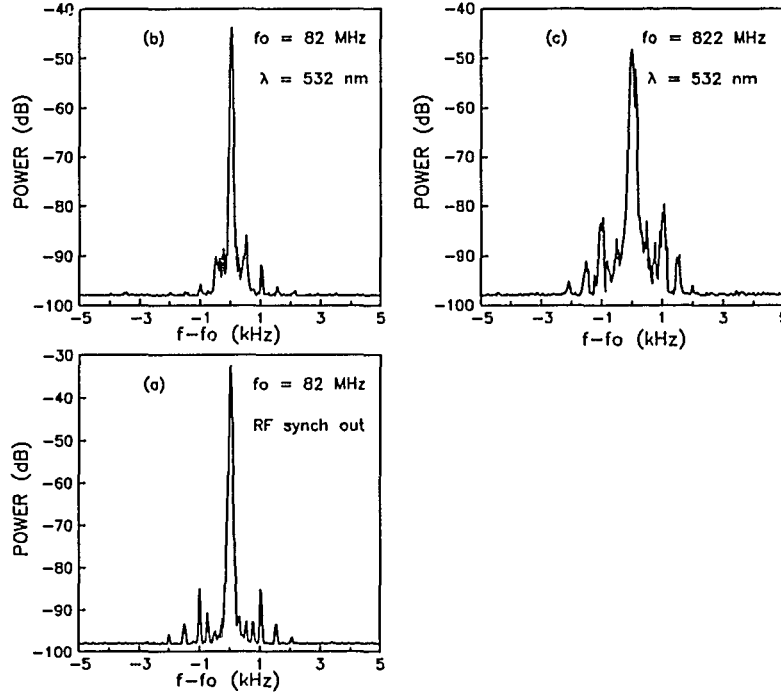


Figure 9. Noise power spectra of (a) the mode-locker synch out signal and (b), (c) the $\lambda = 532$ nm intensity of the Nd:YAG pump laser. The resolution bandwidth is 30 Hz.

This spectrum consists of distinct peaks at multiples of 500 Hz, which are direct consequences of a phase detector in the frequency synthesizer of the mode-locker driver unit that compares and adjusts the RF output signal to a precision reference oscillator signal at 500 Hz rate [Spectra Physics, 1990]. The peaks result from the periodic adjustments of the RF signal driving the mode-locker. These modulations bring about periodic cavity Q changes in the Nd:YAG laser, causing the $\lambda = 532$ nm output power spectra to duplicate the same sharply peaked structure. It should be noted that the theoretical approach depicted in chapter 2.2. is valid for this type of

noise. The only restrictions of the theory are the assumptions of a constant pulse shape and fluctuations that are slowly varying compared to the pulse repetition time. The sinusoidal modulations of the pump laser intensity, represented by the sharp sidebands in the noise spectra, are sufficiently low in frequency to satisfy the assumptions. Between $n = 1$ (82 MHz) and $n = 10$ (822 MHz) the noise bands on both sides of the central peak increase strongly, indicating the presence of a timing jitter. Figure 10 shows the square dependence of the pump laser jitter noise on the order number n for the 1 kHz sidebands. The excellent agreement of the data points with a quadratic function is emphasized by the very small difference between the 6th order polynomial best fit, which has been added for reference (dashed line), and the quadratic best fit (solid line). Using Equation 11, a r.m.s. repetition rate fluctuation of $\Delta T/T = 0.12\%$ is obtained. At 82 MHz this is equivalent to $\Delta T = 15$ ps. This result is supported by direct sampling oscilloscope measurements by Spectra Physics, which showed a r.m.s. timing jitter of 25 ps. The r.m.s. energy fluctuations of the green Nd:YAG pulses are $\Delta E/E = 3\%$ according to Equation 10. In summary, the pump laser carries considerable timing jitter compared to its pulse duration, while its amplitude fluctuations are small.

Next, the dye laser noise is examined. Figures 11 and 12 show the dye laser noise for the $\Delta L = -0.7\ \mu\text{m}$ and $\Delta L = 0$ cases, respectively, in the same frequency span of ± 5 kHz around the 82 MHz and 822 MHz peaks that contained all of the pump laser noise components. Figure 12 exhibits an increase of the noise sidebands for $n = 10$ similar to the pump laser noise, which indicates that the dye laser follows the pump laser in terms of timing jitter. When evaluated in the same way as above, the r.m.s. jitter is $\Delta T = 12$ ps for the $\Delta L = -0.7\ \mu\text{m}$ case. The $\Delta L = 0$ case presents itself slightly differently, as shown in Figure 12, exhibiting a broadband noise pedestal with the familiar narrow sidebands superimposed.

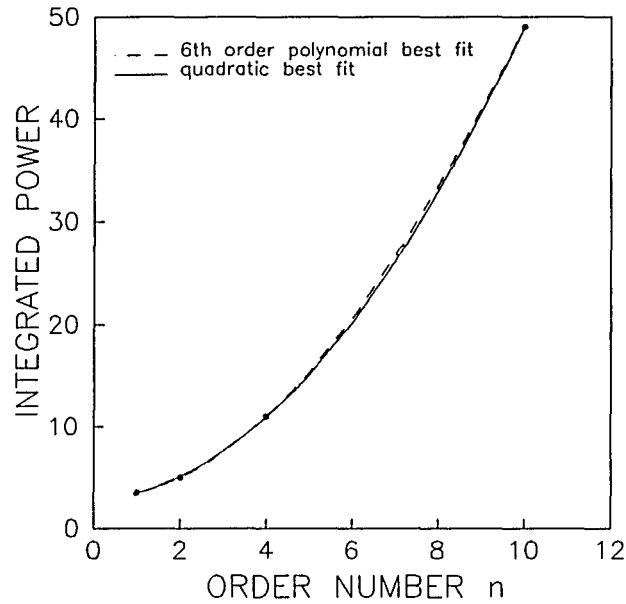


Figure 10. Quadratic fit of the pump laser jitter noise data to the order number n for the 1 kHz sidebands of Figure 9 (solid line). A 6th order polynomial best fit (dashed line) does not agree better with the data, proving that the quadratic fit is sufficient.

Although the 82 MHz and the 822 MHz noise spectra look similar, Equation 11 yields a r.m.s. jitter of $\Delta T = 14$ ps. Within the accuracy of these measurements the dye laser jitter can be attributed to pump laser jitter in both cases. This explanation agrees with previously observed behavior of synchronously pumped dye lasers [Kluge et al., 1988].

In order to estimate the energy fluctuations of the dye laser, a larger frequency span has to be chosen. Unlike the pump laser noise, which is confined within a range of ± 2.5 kHz from each repetition rate multiple, the dye laser noise covers a much broader frequency range of ± 300 kHz. Figure 13 shows a comparison of the amplitude fluctuations of the $\Delta L = 0$ with the $\Delta L = -0.7 \mu\text{m}$ case.

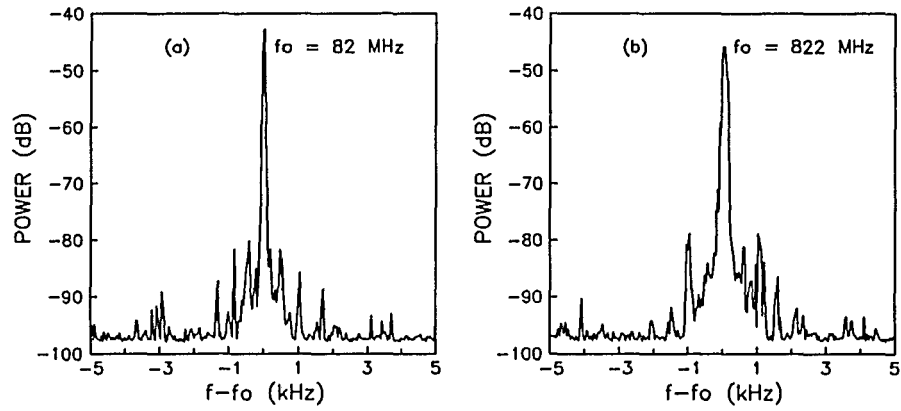


Figure 11. Noise power spectra of the dye laser intensity at $\Delta L = -0.7 \mu\text{m}$. The resolution bandwidth is 30 Hz.

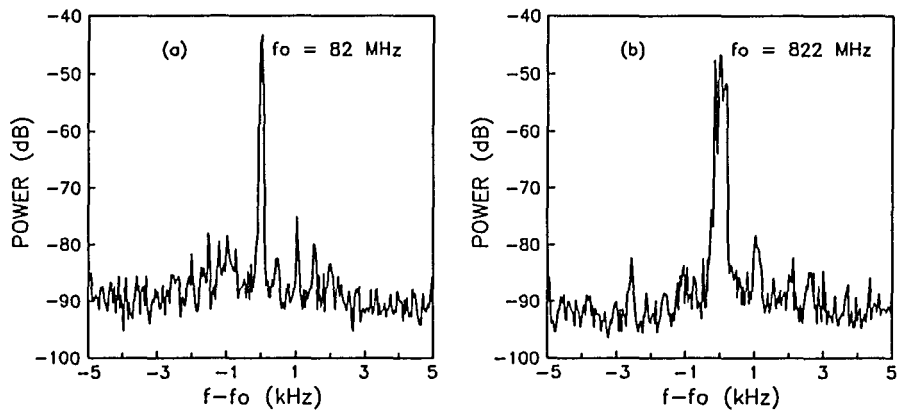


Figure 12. Noise power spectra of the dye laser intensity at $\Delta L = 0$. The resolution bandwidth is 30 Hz.

Applying Equation 10, one finds pulse energy fluctuations of $\Delta E/E = 9\%$ in both cases. Higher order noise spectra do not exhibit any noise increase, signifying no additional timing jitter contributions.

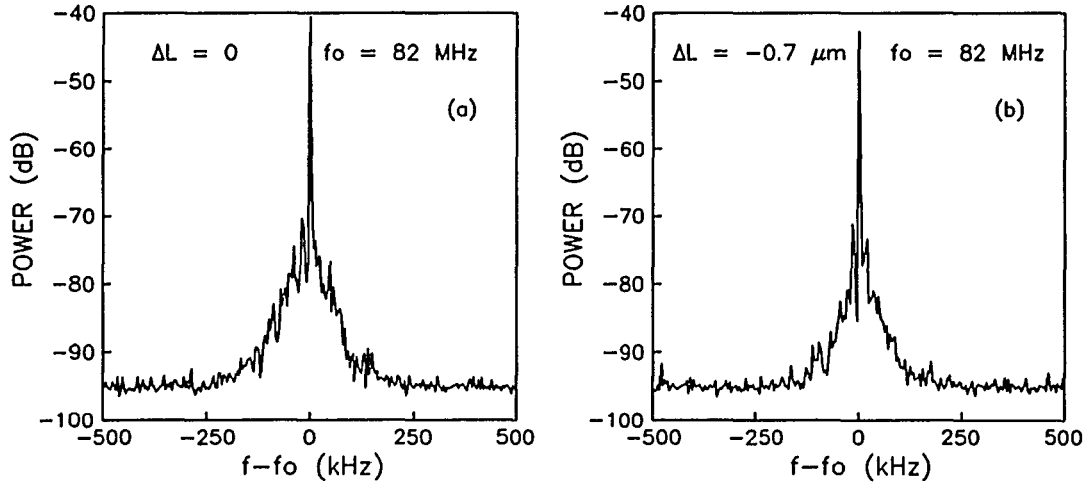


Figure 13. Lower resolution, larger frequency span versions of Figures 12 (a) and 11 (a). The resolution bandwidth is 100 Hz.

The noise burst model predicts pulse energy fluctuations of magnitude $\Delta E/E = (t_n/t_p)^{1/2}$. In both cavity detuning cases the autocorrelations are narrow without "coherence spikes" such that $t_n \approx t_p$, yielding approximately 100 % pulse energy fluctuations. This result shows the inadequacy of the noise burst model for modelling the laser output at small cavity length detunings. Also no shifts between the δ -parts and the centers of the noise bands are present in the power spectra that could justify further consideration of the noise burst model. The absence

of these shifts can be ascribed to the smallness of the cavity length detuning in both cases.

An interesting difference between the energy fluctuations in the two cases is seen better in an intermediate frequency span as shown in Figure 14. The $\Delta L = -0.7 \mu\text{m}$ spectrum has a double-lobed structure with its peaks at about $\pm 25 \text{ kHz}$ away from the center and almost no noise frequency components between them.

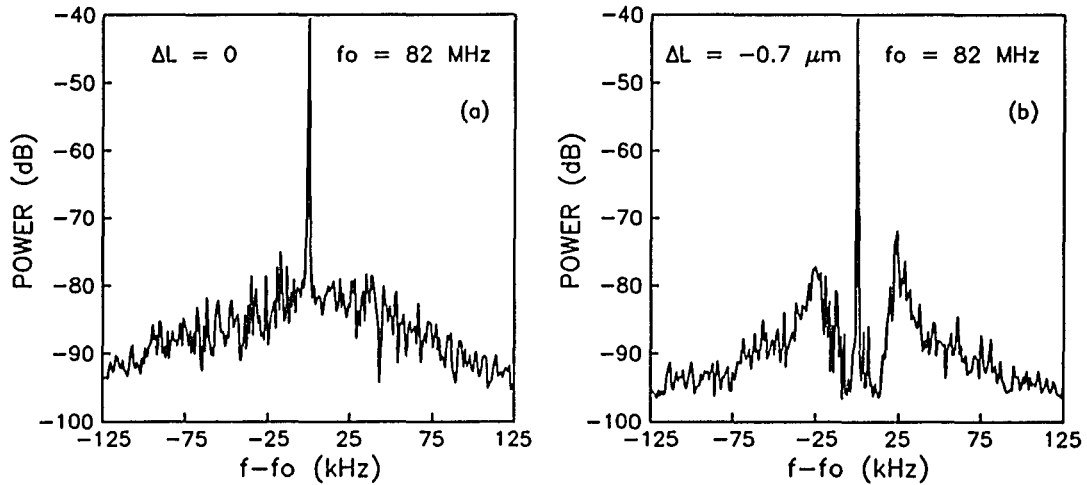


Figure 14. Intermediate frequency span versions of Figures 12 (a) and 11 (a). The resolution bandwidth is 100 Hz.

Similar distinct spectral features appear in the pump laser power spectra that are, however, narrower and located at different frequencies. In this case the 25 kHz oscillation peaks

are broader due to the presence of other noise sources. The side lobes are related to a sinusoidal modulation of the laser output. This can be understood by considering the fact that a sinusoidal amplitude modulation function has a power spectrum with two symmetrically located side peaks, where the distance from the center to each peak equals the oscillation frequency. The detailed structure of these sidepeaks is determined by the envelope of the sinusoidal modulation.

A simple model can explain this behavior as illustrated in Figure 15. Since we observe oscillations of the $\Delta L = -0.7 \mu\text{m}$ pulse train directly in the time domain at the same frequency of approximately 25 kHz, which are not present in the $\Delta L = 0$ pulse train, we assume a sinusoidal function for the random intensity fluctuation function $A(t)$ as shown in Figure 15 (a). Figure 15 (b) shows $G_A(t)$, the autocorrelation of $A(t)$ and the resulting power spectrum $\text{Log}[P_A(\omega)]$ is plotted in Figure 15 (c). The shape of $\text{Log}[P_A(\omega)]$ agrees very well with the measured shape of Figure 15 (b), identifying a plausible explanation for the $\Delta L = -0.7 \mu\text{m}$ power spectra. It should be noted that single sided negative exponential, as well as Gaussian and triangular, envelope functions for $A(t)$ did not give as good an agreement.

The good agreement between the data and our simple model suggests a sinusoidal modulation $A(t)$ which we attribute to self-pulsing [Kühlke, 1985; New and Catherall, 1986] that is interrupted by competing noise mechanisms, such as dye jet inhomogeneity. Self-pulsing develops when a cavity length mismatch prevents the pulse shaping mechanism provided by the gain and absorber media from fully compensating the temporal walk-off of the dye laser pulse with respect to the pump pulse. Eventually the dye laser pulse moves out of the gain window and collapses. Then a new pulse builds up from amplified spontaneous emission. This periodic phenomenon carries random fluctuations due its dependence on spontaneous emission.

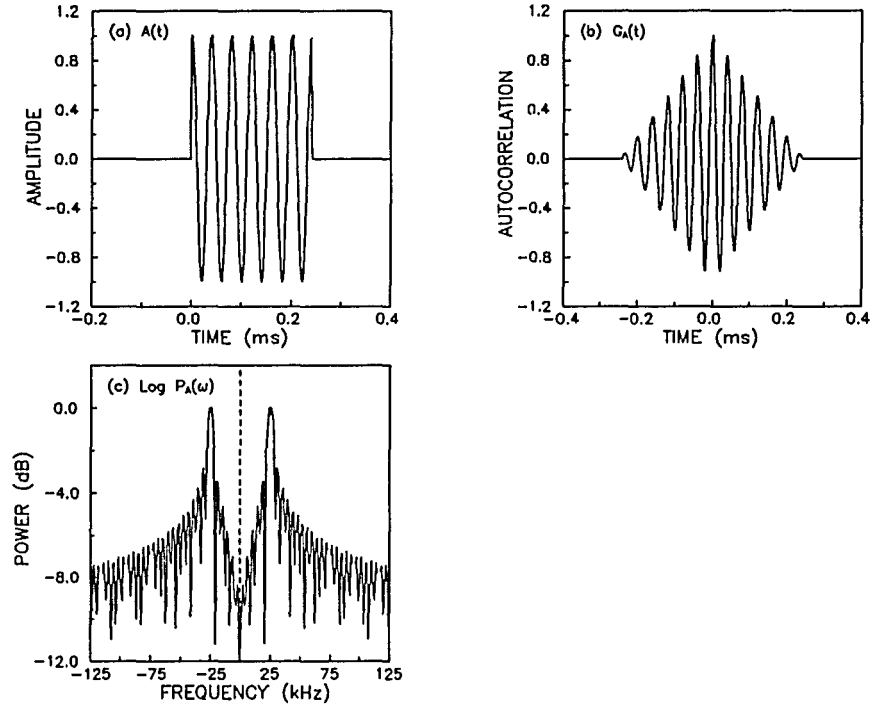


Figure 15. (a) Sample time interval of modelled random amplitude fluctuation function $A(t)$. (b) Autocorrelation $G_A(t)$ of $A(t)$. (c) Logarithm of the normalized power spectrum $P_A(t)$ of $A(t)$. The dashed line has been inserted to mark the central frequency location.

New and Catherall distinguish between $t_m > 0$ self-pulsing and $t_m < 0$ self-pulsing, where $t_m = T_{\text{cav}} - T_{\text{ext}}$ is the difference between the cavity transit time T_{cav} and the pump laser repetition time T_{ext} [New and Catherall, 1986]. They obtain self-pulsing for $t_m > 0$ only when the relaxation time of the laser medium is comparable to T_{cav} while this condition does not apply

to $t_m < 0$. The fluorescent lifetime of our laser dye has been measured to be less than 1 ns [Smith et al., 1984] which is small compared to our $T_{\text{cav}} = 12$ ns. Therefore, we can exclude the $t_m > 0$ case from consideration. This agrees with the fact that we have to shorten our cavity slightly in order to observe the $\Delta L = -0.7 \mu\text{m}$ mode of operation. Self-pulsing is expected to be perturbed by other noise sources in our laser that vary on the same time scale, e. g. dye jet inhomogeneity. This effectively stops self-pulsing and proves reasonable the assumptions made in our simple model explaining the shape of the observed power spectra.

Finally, the pulse duration fluctuations are extracted from the noise spectra of dye laser second harmonic as displayed in Figure 16, utilizing Equation 12. The results are $\Delta t_p/t_p = 21\%$ ($\Delta L = 0$) and $\Delta t_p/t_p = 52\%$ ($\Delta L = -0.7 \mu\text{m}$). Examination of higher order noise spectra shows no timing jitter contributions on this frequency scale. The pulse duration fluctuations are about twice as large in the $\Delta L = -0.7 \mu\text{m}$ case. This agrees with the lower autocorrelation peak: An average over pulses of different duration, but roughly the same pulse energy yields a reduced peak intensity and a broader shape compared to an average over the shortest pulses. The larger pulse width fluctuations in the $\Delta L = -0.7 \mu\text{m}$ case are another piece of evidence for the presence of self-pulsing. The calculations of New and Catherall [New and Catherall, 1986] clearly show such large fluctuations.

2.4. Conclusion

Two distinct modes of operation of a femtosecond synch-pumped dye laser under study have been identified and characterized. Timing jitter, pulse energy and pulse duration

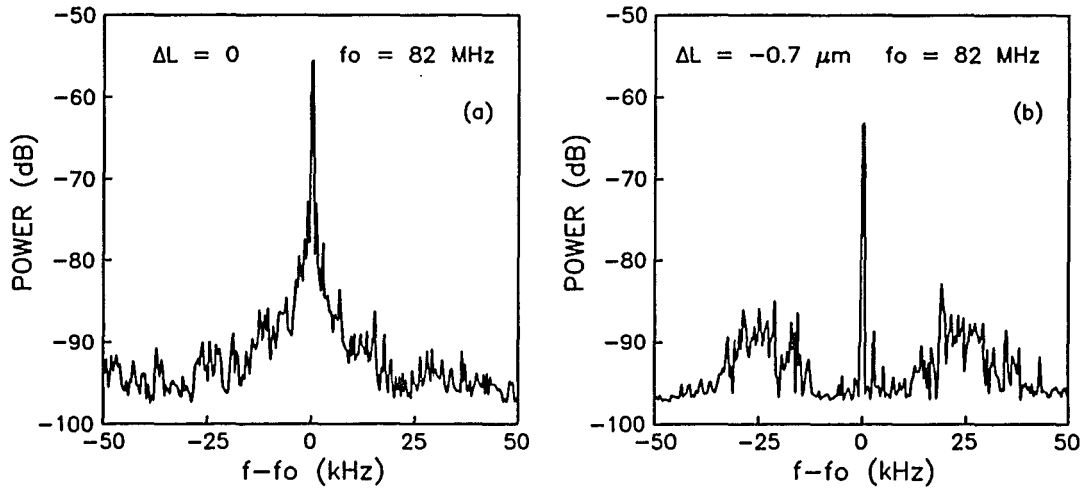


Figure 16. Noise power spectra of dye laser second harmonic intensity. The resolution bandwidth is 100 Hz.

fluctuations have been investigated. The timing jitter has been ascribed to the timing jitter of the pump laser, which, in turn, has been linked to electrical noise in the mode-locker driver. The pulse energy fluctuations are similar in both modes of operation, whereas the shapes of the respective noise spectra differ distinctly. The $\Delta L = -0.7 \mu\text{m}$ case has distinct noise peaks at ± 25 kHz off center and shows corresponding oscillations in its pulse train envelope. In addition, it exhibits pulse duration fluctuations that are twice as strong as in the $\Delta L = 0$ case. The noise power spectrum can be explained by a simple model based on chopped sinusoidal modulations. This evidence points toward a form of self-pulsing that is interrupted by competing

noise mechanisms, such as dye jet inhomogeneity.

Contrary to a naive interpretation of the autocorrelation measurements, it seems that the $\Delta L = -0.7 \mu\text{m}$ case is less useful for time resolved ultrafast experiments, because its pulse duration is not well defined. In general, the stability of this laser system leaves much to be desired, unless sophisticated active stabilization schemes are employed. Fortunately in many cases, these systems may be replaced by much simpler mode-locked Ti:Sapphire lasers [Spence et al., 1991] that promise to deliver more stable femtosecond pulses in the near infrared and, frequency doubled, in the blue spectral region.

CHAPTER 3

NONLINEAR DIRECTIONAL COUPLER

3.1. Introduction

All-optical switching in nonlinear optical devices is of considerable interest for very high bandwidth optical communication applications. These devices would be very useful at the input and output ends of the now common fiber-optic transmission systems. If nonlinear materials with sub-picosecond response times were utilized, all-optical devices could surpass the signal processing speed of electronic switches. Then photonic devices could be competitive with electronics even for transmission and connection tasks involving signal propagation distances as short as 1 cm [Kogelnik, 1992].

Picosecond all-optical switching, based on bandgap resonant nonlinearities, has been demonstrated in semiconductor doped glass [Finlayson et al., 1988] and GaAs/AlGaAs multiple quantum well directional couplers [Jin et al., 1988; LiKamWa et al., 1990] using pump-probe techniques. These devices all relied on the generation of a high enough charge carrier concentration to bleach the exciton absorption peaks. The recovery times were therefore determined by the recombination time of these carriers. LiKamWa et al. recently improved the recovery time of their "zero gap" waveguide switch to 130 ps by the application of an electric field to accelerate the carrier sweep-out [LiKamWa et al., 1991]. The zero gap structure is single mode in the quantum well growth direction, but supports two lowest lateral modes in the transverse direction perpendicular to the growth direction. These modes beat with each other

during propagation, behaving similar to the two separate waveguides of a directional coupler, if the output is detected close to the end facet. This near field output pattern was switched from an initial ratio of 7:1 between the peak intensities of the two modes to 1:7.

Femtosecond all-optical switching has been shown in a fused quartz dual-core optical fibers [Friberg et al., 1988] and GaAs/AlGaAs multiple quantum well waveguides [LaGasse et al., 1989; Sokoloff et al., 1989; Lee et al., 1991]. The nonlinearity exploited in the dual-core fiber directional coupler switch of Friberg et al. is the Kerr effect, as evidenced by the accurate theoretical simulation of the output vs. input power characteristic and the observation of the expected pulse breakup due to the Kerr effect. For a single input pulse with a peak power that exceeds the switching threshold only the most intense, central portion switches, leaving the less intense leading and trailing edges behind. One output port then transmits the peak of the pulse, while the other delivers the leading and trailing edges, generating the triple-peaked autocorrelation functions that were measured. The autocorrelations of the switched transmitted pulse peaks were almost identical to those of the input pulses. La Gasse et al. studied all-optical switching in a single AlGaAs ridge waveguide using time division interferometry. This extension of the pump-probe technique employs a third (reference) pulse that is temporally advanced with respect to the pump and probe pulses before entering the waveguide. After passage through the sample the delay between reference and the probe pulses is removed and the resulting interference signal is detected. This permits measurements of amplitude and phase of the transmitted probe pulses. The femtosecond switching results, obtained under below-resonance excitation, showed a transient response that followed the pulse duration of about 400 fs and a long-lived response, which was attributed to the presence of charge carriers. Two-photon absorption was identified as the dominant carrier generation mechanism by a transient absorption measurement that showed a decrease in the probe transmission only during the pump pulse.

The rest of this chapter describes in detail the all-optical switching results in quantum well directional couplers identical to the ones of Jin et al. [Jin et al., 1988], but using femtosecond pulses [Harten et al., 1990]. The necessary ultrafast refractive index modulation is identified as a property of the optical Stark effect [Fröhlich et al., 1986; Mysyrowicz et al., 1986; Peyghambarian et al., 1989]. This interpretation is supported by an increase of the total transmission through the device, which arises from the transient shift and bleaching of the exciton resonance during the presence of the pump pulse.

3.2. The directional coupler device

A directional coupler comprises a pair of closely spaced waveguides. The spacing between them and their respective mode structure determine how much of the evanescent tails of the light electromagnetic fields propagating along each waveguide can penetrate into the other. This evanescent coupling can initiate a periodic light exchange between the guides which is very similar to the periodic energy exchange between two coupled pendula. Following Lee's treatment of the coupled mode formalism [Lee, 1986] the electromagnetic fields in a directional coupler can be expanded in terms of the modes of each waveguide, when it is isolated from the other waveguide. For waveguides which each support single transverse modes this approximation yields:

$$\vec{E}(\vec{r}) = a_A(z) \vec{E}_A(x,y) e^{-ik_A z} + a_B(z) \vec{E}_B(x,y) e^{-ik_B z} . \quad (13)$$

$$\vec{H}(\vec{r}) = a_A(z) \vec{H}_A(x,y) e^{-ik_A z} + a_B(z) \vec{H}_B(x,y) e^{-ik_B z} . \quad (14)$$

Here \vec{E} and \vec{H} are the electromagnetic fields in the directional coupler, \vec{E}_A , \vec{H}_A , and \vec{E}_B , \vec{H}_B , are the single mode transverse electromagnetic field distributions in waveguide A and B without interaction, respectively, $k_{zA} = (2\pi/\lambda_A)\cos\theta_A$ and $k_{zB} = (2\pi/\lambda_B)\cos\theta_B$ are the projections of the wavevectors onto the z axis (the angles θ_A and θ_B are measured from the z axis to the wavevectors) in guide A and B, respectively, and the expansion coefficients a_A and a_B remain to be determined by the following set of coupled differential equations

$$\frac{da_A}{dz} = -ia_B C_{BA} e^{i\Delta kz}, \quad (15)$$

$$\frac{da_B}{dz} = -ia_A C_{AB} e^{i\Delta kz}, \quad (16)$$

where $\Delta k = k_{zA} - k_{zB}$; C_{AB} and C_{BA} are overlap integrals that involve \vec{E}_A , \vec{E}_B , and the dielectric constant differences between the guiding regions and the cladding material. Under phase-matched conditions ($k_{zA} = k_{zB}$), which are satisfied for identical waveguides, the problem collapses into that of simple harmonic oscillators. Then the overlap integrals C_{AB} and C_{BA} become identical

$$C_{AB} = C_{BA} = C = \frac{\omega}{2} \iint \Delta\epsilon |\vec{E}_A(x,y) \cdot \vec{E}_B(x,y)|^2 dx dy. \quad (17)$$

where ω is the angular light frequency, and $\Delta\epsilon$ is the dielectric constant difference between core and cladding. The set of differential equations for the coupling coefficients now becomes

$$\frac{da_A}{dz} = -ia_B C, \quad (18)$$

By inserting Equation 18 into Equation 19 the harmonic oscillator equation is obtained:

$$\frac{da_B}{dz} = -ia_A C . \quad (19)$$

$$\frac{d^2 a_A}{dz^2} + C^2 a_A = 0 . \quad (20)$$

The resulting sinusoidal dependence of the electromagnetic fields on the propagation distance z yields the periodic energy exchange between the waveguides. If the light is initially coupled only into waveguide B, the guided optical powers P_A and P_B are

$$P_A(z) = \sin^2(Cz) , \quad (21)$$

$$P_B(z) = \cos^2(Cz) . \quad (22)$$

The propagation distance $z_0 = \pi/(2C)$ of complete power transfer from the initial waveguide into the other, which determines the size of the actual device, is called coupling length. Practical implementations rely on externally or internally perturbing the material in one of the waveguides to generate a nonlinear electric polarization, which creates a nonlinear phase-mismatch between the waveguides, and prevents the light transfer after a propagation distance z_0 . In the present case the directional coupler consists of a $1.2 \mu\text{m}$ thick nonlinear guiding region of 100 \AA GaAs/ 100 \AA AlGaAs multiple quantum wells that is sandwiched between two AlGaAs cladding layers of lower refractive index for vertical confinement of the guided light. Horizontal confinement is achieved by ridges formed in the top cladding layer by reactive ion etching. The device length is 1.24 mm , close to the theoretically estimated coupling length of about $z_0 = 1 \text{ mm}$ [Chuang, 1991]. The dielectric constant is perturbed here by an intense, below-resonance,

light pulse that temporarily modifies the optical properties of the semiconductor bandedge. In the unperturbed state most of the light transfers over from the initial into the adjacent waveguide. In the perturbed, nonlinear state the coupling length is extended so much that most of the light stays in the initial waveguide. A cross sectional view of the sample is shown in Figure 17.

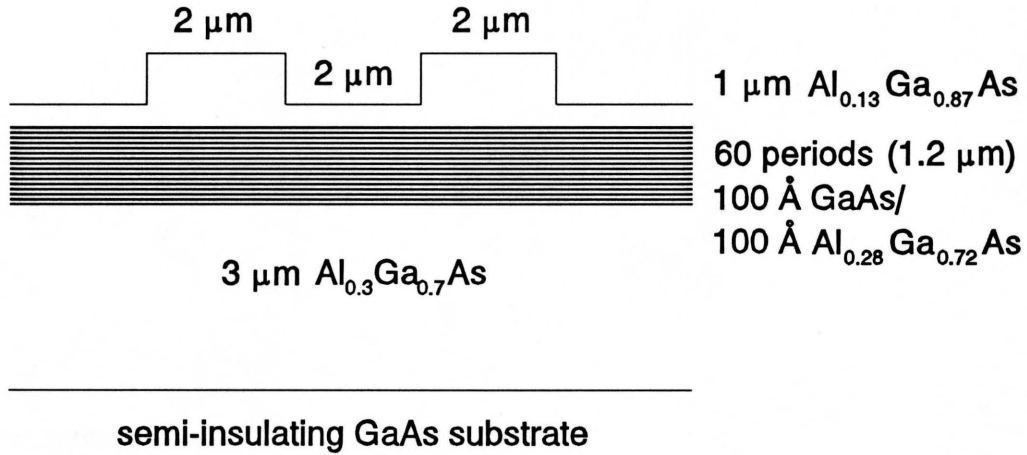


Figure 17. Cross section of nonlinear directional coupler design.

3.3. Experimental setup

For this experiment the unamplified dye laser beam is acousto-optically chopped to avoid heat-induced, slow-response-time, thermal nonlinearities in the waveguides. The pulses are temporally broadened, mainly by the acousto-optic modulator, from a 100 fs FWHM at the dye

oscillator to a 300 fs FWHM at the waveguide. A half-wave plate with a polarizing beamsplitter (PBS) provides two beams with orthogonal polarizations and adjustable intensity ratio. The more intense, vertically polarized pulses serve as pump beam, generating the main portion of the nonlinear effect, while the less intense, horizontally polarized pulses act as probe beam. The time delay $\Delta t = t_{\text{probe}} - t_{\text{pump}}$ is adjusted by a stepper-motor-controlled delay line that varies the optical path length of the pump pulse. Both beams are collinearly endfire-coupled into the same waveguide input channel. The probe pulses, which monitor the pump-induced changes in the device, are detected at the output end, where the pump beam is diverted. The experiment is schematically pictured in Figure 18.

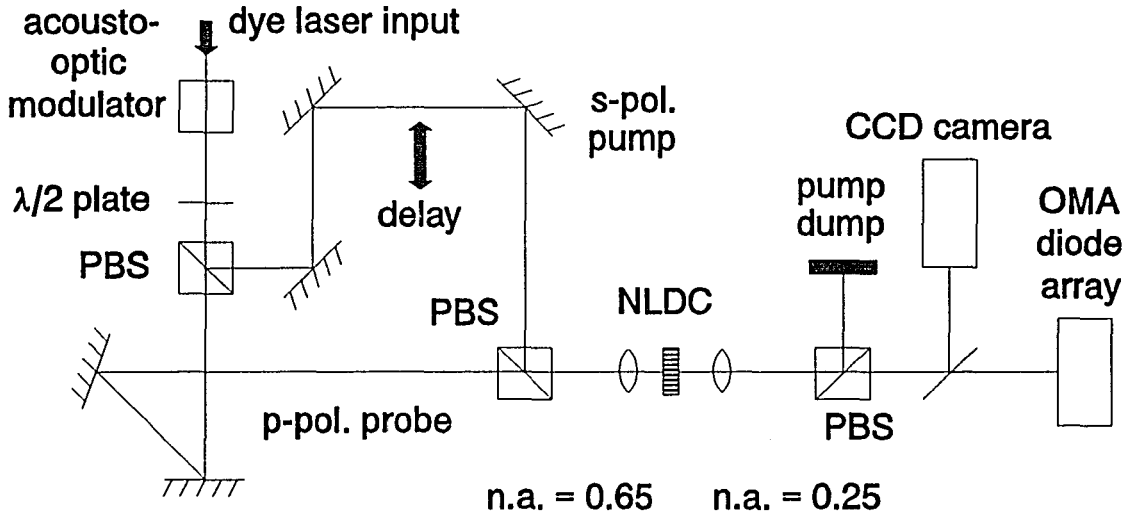


Figure 18. Configuration of nonlinear directional coupler (NLDC) all-optical switching experiment. PBS: Polarizing beam splitter.

The distinct polarization dependence of the optical response of multiple quantum well structures [Weiner et al., 1980] is employed in this experiment to optimize the effectiveness of pump and probe pulses in their respective assignments. The polarizations of the pump and the probe beams are chosen perpendicular and parallel to the multiple quantum well planes, respectively. As a result of this choice, the detuning of the pump pulse from the onset of absorption (light-hole exciton transition in this case) is 37 meV. The detuning of the probe from the absorption edge (heavy-hole exciton in this case) is only 28 meV, although pump and probe have identical wavelengths. The larger detuning of the pump pulse reduces the number of real carriers generated by absorption and, therefore, minimizes the unwanted nonlinearities due to an electron-hole plasma with a recombination time of several nanoseconds [Chuang, 1991; Jin et al., 1988]. The magnitude of the absorption coefficient is roughly 26 cm^{-1} in the spectral band of interest around $\lambda = 870 \text{ nm}$ [Jin et al., 1990].

3.4. Observation of femtosecond all-optical switching

In Figure 19 the complete switching characteristic of the device is displayed by plotting probe beam transmission profiles through the directional coupler as a function of time delay Δt . These transverse spatial profiles are recorded by imaging the output facet onto a linear photodiode array. The insert in Figure 19 diagrams the two routes a pulse can take throughout the device: If it is injected into one waveguide it may then either shift over into the other (linear propagation) or stay in the initial channel (nonlinear regime). The main segment of Figure 19 starts at negative time delays $\Delta t < 0$, where the probe pulse precedes the pump pulse. At $\Delta t = -500 \text{ fs}$ the probe pulse crosses over from the input waveguide (channel 2) to the other (channel 1). Around $\Delta t = 0$ both pulses overlap temporally and the probe switches back to the

input channel 2. A close inspection reveals that the total probe transmission, integrated over the whole transmission profile (both channels), increases. For $\Delta t > 0$ the transmission profile almost returns to its initial shape, indicating ultrafast recovery within about 300 fs.

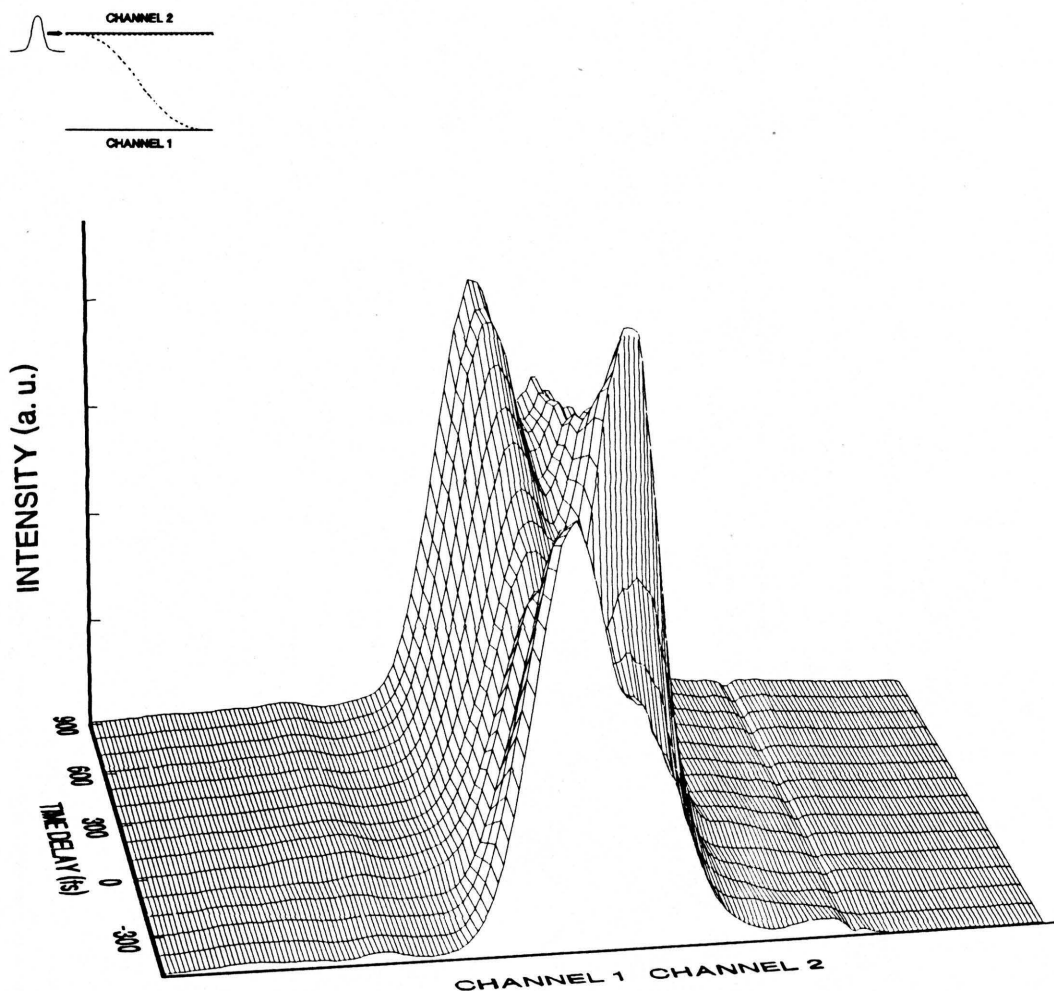


Figure 19. Transmitted probe beam profiles as a function of time delay Δt . The profiles are intensity scans across the image of the output facet of the nonlinear directional coupler. The inset schematically shows how the light is inserted into and propagates through the device with and without nonlinearly modified coupling between the waveguides.

In Figure 20 the first half of the switching characteristic of Figure 19 is displayed differently by plotting the normalized transmissions of the probe beam through both channels of the device as functions of the pump intensity for the time delay range $\Delta t = -500$ fs to $\Delta t = 0$. In calculating the pump intensities the pulse duration increase from about 100 fs at the oscillator to about 300 fs at the position of the nonlinear directional coupler has been taken into account. The relative transmission of a directional coupler channel is defined here as its transmission divided by the total transmission of both channels. The cross-over point between the relative transmissions of the two channels provides a lower limit for the pump intensity required to switch I_s . This cross-over occurs at $I_s = 2$ GW/cm² in Figure 20.

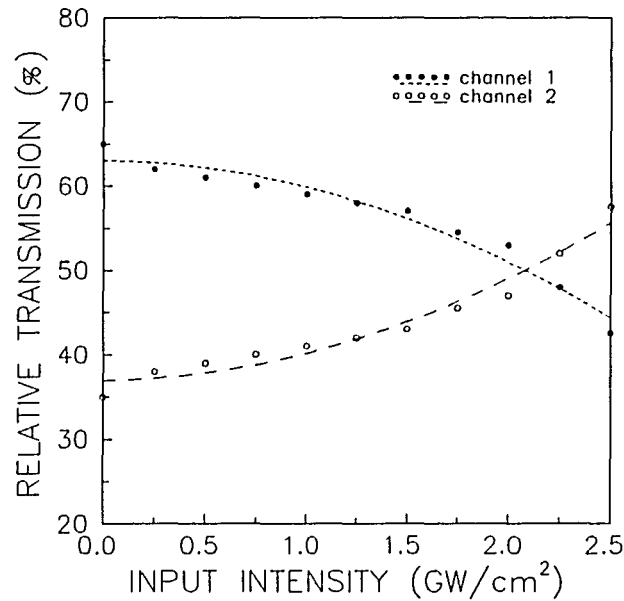


Figure 20. Relative probe transmission as a function of pump intensity for both coupler channels. Pump and probe beams are injected into channel 2. The dashed lines are guides to the eye.

Figure 21 displays the total probe beam transmission versus time delay Δt as defined earlier in this chapter, and normalized to its peak value. An extremely fast transmission increase around $\Delta t = 0$ is clearly noticeable. Most of this increase recovers quickly with a decay time of about 200 fs. The small remaining component which recovers slowly on this time scale can be explained by the presence of a real charge carrier population. The lifetime of this electron-hole plasma is approximately 4 ns, limited by recombination [Chuang, 1991]. During this time the exciton resonance will remain somewhat bleached, keeping the transmission at the observed, slightly increased level [Park et al., 1988]. The rapid oscillations in Figure 21 are caused by interference of a very small portion of the pump beam that is polarized in the probe beam polarization direction due to imperfections in the polarizing optics.

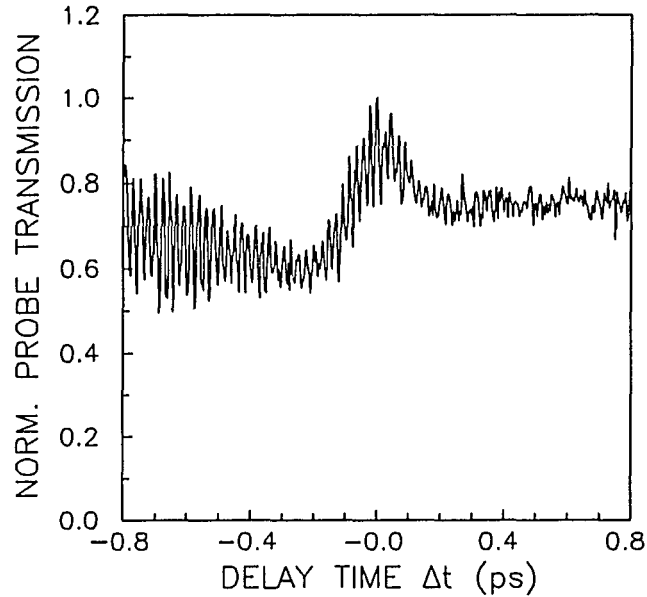


Figure 21. Total probe beam transmission, normalized to its peak value, versus time delay Δt .

The real carrier population can in principle originate from either one-photon absorption associated with the tail of the exciton line or two-photon absorption of conduction band states. The dependence of the slowly recovering feature on the pump intensity may help distinguishing between these two excitation mechanisms. For this purpose consider the output peaks of each channel in Figure 19 at large negative and large positive time delays. It is possible to define the lack of recovery for a directional coupler channel as the difference between its relative transmissions at $\Delta t = -1$ ps and at $\Delta t = +1$ ps. In Figure 22 the lack of recovery is plotted against the pump intensity.

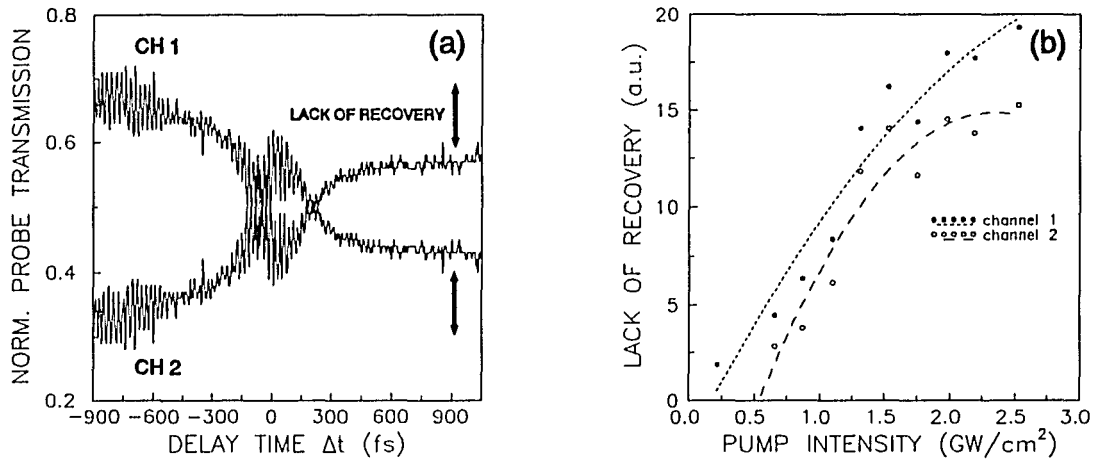


Figure 22. (a) Relative probe beam transmission as a function of time delay Δt . In contrast to Figure 19, where spatial profiles are plotted at discrete time intervals, here the spatially integrated outputs are plotted as continuous functions of time for each channel. (b) Lack of recovery, as explained in the text and shown in part (a) of this figure, versus pump intensity. The dashed lines are guides to the eye.

Figures 19, 21, and 22 (a) evidence that the lack of recovery is much smaller than the ultrafast part of the switching characteristic. This implies that the absolute number of real carriers generated here is small compared to the number of carriers required for real carrier-induced switching, which has been demonstrated first by Jin et al. in this device, using picosecond light pulses [Jin et al., 1988]. The relative probe transmission curves as a function of pump intensity measured by Jin et al. may be approximated as straight lines in the limit of small carrier densities. Then the lack of recovery should depend linearly on the pump intensity for one-photon absorption, but quadratically for two-photon absorption. Figure 22 (b) contradicts the two-photon absorption hypothesis by displaying a linear increase and even saturation for high intensities, making two-photon absorption irrelevant under these circumstances.

3.5. Adiabatic following and optical Stark effect in semiconductors

The recent progress in semiconductor physics makes it possible to theoretically model the microscopic dynamics of optical excitations in these materials [Schmitt-Rink et al., 1985; Fluegel et al., 1987; Koch et al., 1988; Schmitt-Rink et al., 1989; Haug and Koch, 1990]. Under certain approximations, namely the two-band model for the semiconductor electron-hole system and the Hartree-Fock approximation for the coupling to the quantized electromagnetic field, one can derive a set of coupled equations, known as the semiconductor Bloch equations [Lindberg and Koch, 1988]. Analogous in formal structure and in substance to the Bloch equations for atomic systems the semiconductor Bloch equations describe the interaction between light and matter.

$$\begin{aligned}
(i\hbar \frac{\partial}{\partial t} + \frac{i\hbar}{T_2} - e_{\vec{k}} + 2 \sum_{\vec{k}' \neq \vec{k}} V_{\vec{k}-\vec{k}'} f_{\vec{k}'}) P_{\vec{k}} = \\
= - (1-2 f_{\vec{k}}) (\sum_{\vec{k}' \neq \vec{k}} V_{\vec{k}-\vec{k}'} P_{\vec{k}'} + \vec{\mu} \vec{E}) , \quad (23)
\end{aligned}$$

$$\hbar \frac{\partial}{\partial t} f_{\vec{k}} = 2Im[(\sum_{\vec{k}' \neq \vec{k}} V_{\vec{k}-\vec{k}'} P_{\vec{k}'}^* + \vec{\mu}^* \vec{E}^*) P_{\vec{k}}] . \quad (24)$$

where $e_{\vec{k}} = E_g + \hbar^2 k^2 / (2m) - \hbar \omega_L$, $E_g + \hbar^2 k^2 / (2m)$ is the energy of an electron in the conduction band, and $\hbar \omega_L$ is the center energy of the light. Here T_2 is the polarization dephasing time, V is the Coulomb potential, f is the electron density, d_{cv} is the dipole interband matrix element, P is the interband polarization, and E is the electric field amplitude in the rotating frame. These equations describe coherent processes that take place within the polarization dephasing time of the material, as well as incoherent, quasi-equilibrium processes that occur after the excited particles have relaxed within their bands from the initial nonthermal energy distributions into quasi-Fermi distributions. The polarization dephasing times are very short in semiconductors, e. g. its upper limit in GaAs at room temperature is given by the exciton ionization time of 400 fs [Peyghambarian et al., 1984; Schmitt-Rink et al., 1989]. Therefore, coherent effects at room temperature require femtosecond light pulses with a FWHM duration of less than 400 fs.

In the present experiment the excitation is below-resonance with respect to the semiconductor bandgap. This regime is known in atomic physics as adiabatic following [see, e. g., Allen and Eberly, 1975] and has recently been identified in semiconductors [Binder et al., 1990a; Binder et al., 1991]. Under adiabatic following excitation conditions the light pulse varies

sufficiently slowly so that the induced changes in the medium duplicate its time dependence. A more quantitative condition for this regime is the following [Binder et al., 1991]. Adiabatic following arises, whenever the frequency detuning with respect to the closest resonance is larger than the frequency given by the inverse of the characteristic time of the light-induced changes in the medium. This definition is consistent with the one given by Allen and Eberly [Allen and Eberly, 1975].

The same excitation conditions can also be described in the framework of the optical Stark effect [Joffre et al., 1988; Binder et al., 1991]. Similar to the Stark effect in atomic systems the presence of a strong electric field, in this case the electromagnetic light wave, perturbs the energy level structure of the medium. For the present case the semiconductor Bloch equations that describe the light-matter interaction are of course invariant under the label change from "adiabatic following" to "optical Stark effect". In general, however, the optical Stark effect is not limited to the adiabatic following conditions, but can also occur under resonant excitation [Hirlimann et al., 1989].

Since its first experimental observation in semiconductors [Fröhlich et al., 1986] this effect has attracted much attention due to its potential applications in ultrafast optical switching devices [Mysyrowicz et al., 1986; Von Lehmen et al., 1986; Fröhlich et al., 1987; Peyghambarian et al., 1989; Joffre et al., 1989; Knox et al., 1989; Lee et al., 1991; Binder et al., 1991]. Under off-resonance excitation, a transient, so-called virtual charge carrier population is created that exists only during the presence of the optical pulse. A small number of real carriers remains after the pulse, which is due to Coulomb effects and the finite polarization dephasing time. The characteristics of the optical Stark effect, which follow directly from numerical evaluation of the semiconductor Bloch equations [Lee et al., 1991], also include a

transient shift of the excitonic absorption feature to shorter wavelengths (blue-shift) and a transient loss of oscillator strength (bleaching). The results of section 3.4. are well explained based on these properties; i. e. the rapid energy transfer between the waveguides, as seen in Figure 19, is completed within the duration of the pump pulse, indicating an ultrafast refractive index modulation. Such a refractive index change can be linked to the blue-shift of the excitonic absorption feature predicted for the optical Stark effect. The transient transmission increase of the directional coupler, displayed in Figure 21, is consistent with the temporary blue-shift and bleaching of the exciton, providing further evidence for the optical Stark effect hypothesis. The almost complete recovery of the device within the cross-correlation time of pump and probe pulses is also compatible with the calculations of the adiabatic following/optical Stark effect in semiconductors, which predict that the majority of the excited carriers are virtual, and only a small number of real carriers remain.

The results of such a calculation using the semiconductor Bloch equations (Equations 23 and 24) are shown in Figure 23 [Binder et al., 1990b]. In this example, a 50 Å multiple quantum well with an exciton linewidth of $1.2 E_R$, a pump detuning of $10 E_R$, and a Gaussian pump pulse with a peak intensity of 1 GW/cm^2 have been assumed, where E_R is the exciton Rydberg energy. Figure 23 (a) displays the shape of the exciton absorption for different time delays Δt ; Figure 23 (b) depicts the corresponding carrier density and pump pulse intensity temporal profiles. The $\Delta t = -250 \text{ fs}$ (short-dashed) curve in Figure 23 (a) exhibits a the blue-shift of the exciton peak with respect to the linear absorption (solid line). At $\Delta t = 0$ (dotted line), while the exciton peak is still blue-shifted, it is also bleached. The $\Delta t = 250 \text{ fs}$ curve (long-dashed line) closely resembles the linear absorption, signifying an almost complete recovery. The carrier density evolution (solid line) in Figure 23 (b) underscores this point, showing that only a negligible amount of real carriers remains following the pump pulse (dashed

line).

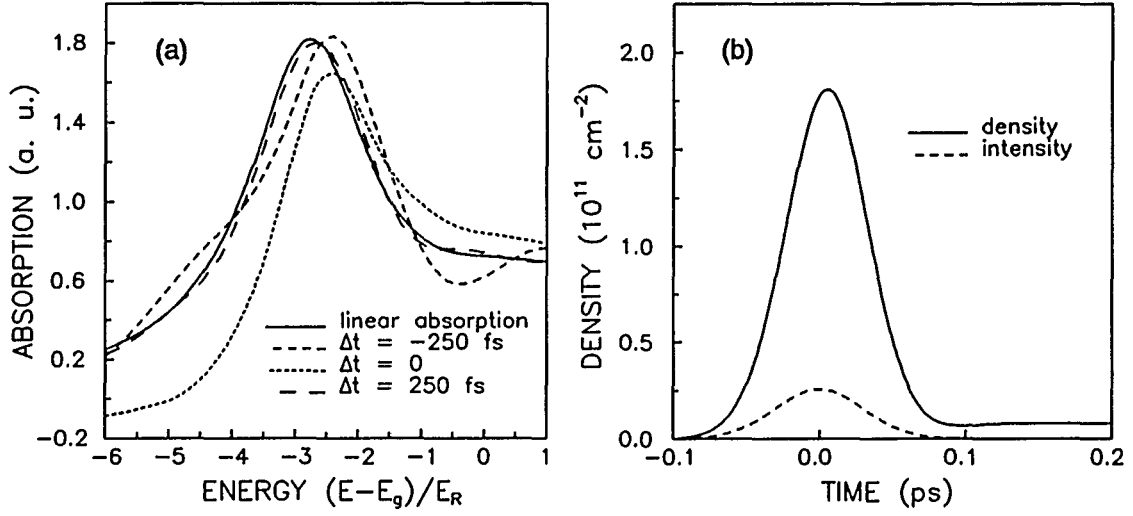


Figure 23. (a) Calculated dynamic change of the excitonic absorption in a 50 Å multiple quantum well under intense (1 GW/cm²), below-resonance, femtosecond excitation. Solid line: linear absorption (no pump), short-dashed line: Δt = -250 fs, dotted line: Δt = 0, long-dashed line: Δt = 250 fs. (b) Temporal profiles of the carrier density (solid line) and the pump pulse (dashed line). E_R is the exciton Rydberg energy, E_G is the bandgap energy.

3.6. Conclusion

A GaAs/AlGaAs multiple quantum well directional coupler has been demonstrated to exhibit femtosecond all-optical switching under off-resonance room temperature excitation in a pump-probe experimental configuration. The ultrafast refractive index change necessary for all-

optical switching in this device is identified as a result of the optical Stark effect. The main obstacle regarding practical applications is the relatively low throughput: The absorption coefficient-propagation length product for this experiment is $\alpha L \approx 3$. Studies with electrically pumped semiconductor waveguides (laser diode amplifiers) to improve throughput have so far not yielded satisfactory results [Chuang, 1991], but are still in progress.

CHAPTER 4

SINGLE WAVEGUIDE COHERENT PULSE PROPAGATION

4.1. Introduction

The nonlinear directional coupler experiment of chapter 3 demonstrates femtosecond switching limited by the cross-correlation time of the pump and the probe pulses, but provides no information about the detailed temporal shape of those pulses. In particular, a possible pulse breakup could have considerable impact on the practical usefulness of such a device. Friberg et al. observed Kerr effect-induced pulse breakup in their dual-core fiber nonlinear directional coupler, as described in chapter 3. In semiconductor directional couplers irradiated with photon energies close to the bandgap energy pulse breakup could occur in a similar way, if the nonlinearity is instantaneous and governed only by the light intensity. If, however, the dependence of the nonlinearity on the light field is more complicated, no such simple prediction can be made. Since pulse breakup in semiconductor waveguides had not been investigated experimentally before, we decided to study the propagation effects of near-resonant, femtosecond light pulses first without the additional complication of evanescent coupling between adjacent waveguides. This situation is examined in the present chapter.

For the experiments considered here the pulse duration is shorter than the polarization dephasing time of the medium. Then the interaction is coherent in the sense that the induced polarization of the material remains in a well-defined phase relationship with the inducing light field during the presence of the pulse. Coherent pulse propagation including self-induced

transparency and pulse breakup in passive atomic media have been studied extensively [McCall and Hahn, 1967 and 1969; Slusher and Gibbs, 1972; Grischkowsky et al., 1973]. However, such coherent processes have only recently been considered for semiconductors where the phase relaxation times are very short and the band structure often prevents the study of a single isolated electronic transition [Becker et al. (1988), Watanabe et al., 1989]. Becker et al. had to use 6 fs pulses to resolve the polarization dephasing times of GaAs band-to-band transitions that ranged between 14 fs and 44 fs, depending on the electron-hole plasma density. Under the experimental conditions of chapter 3 with a detuning of ten bulk exciton Rydberg energies between the light and the closest (1s) exciton the optical Stark effect should produce an ultrafast change in the nonlinear refractive index with a response time (i. e. recovery time) limited only by the polarization dephasing time. This intensity dependent refractive index change is negative and could, in principle, serve to compensate the normal dispersion in this spectral region, allowing a soliton-like pulse propagation.

4.2. Experimental setup

With the experimental setup shown in Figure 24 information can be acquired about the temporal, as well as the spectral shapes of the transmitted pulses. The temporal resolution is provided by a standard cross-correlator, as described by Rothenberg and Grischkowsky [Rothenberg and Grischkowsky, 1989]. In the cross-correlator the incoming amplified dye laser beam is split into a specimen beam and a reference beam. The specimen beam passes through the waveguide while the reference beam travels directly to the nonlinear crystal that provides the cross-correlation signal by sum-frequency generation. The reference beam path includes a telescope which ensures complete spatial overlap between the reference beam and the specimen

beam focal spots. The waveguide output can be directed into a spectrometer for spectral measurements by means of a removable mirror. Figure 25 displays the sample design which is identical to the directional coupler. Note that by supporting a single transverse guided mode this structure performs an automatic spatial filtering operation on the specimen beam.

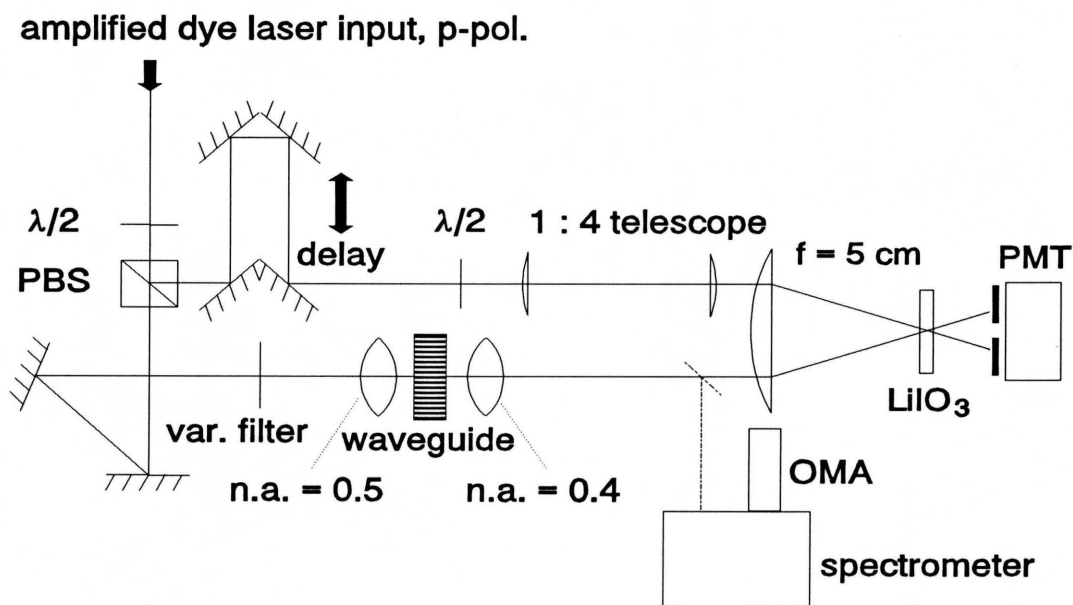


Figure 24. Cross-correlator setup.

The properties of the input pulse train are depicted in Figure 26. Graph 26 (a) is an autocorrelation of the amplified dye laser pulse train before it enters the optics used to couple into the waveguide. The spiked character of the trace originates from the fact that it is sampled by separate pulses. At 1 kHz pulse repetition rate and about 10 Hz autocorrelation recording rate

this sampling is time resolved and shows each pulse. The 150 fs FWHM translates into a FWHM pulse duration of about $t_p = 100$ fs. Together with the spectral FWHM of $\Delta\lambda = 5$ nm of Figure 26 (c) this yields a time-bandwidth product $\Delta\nu \cdot t_p = 0.2$.

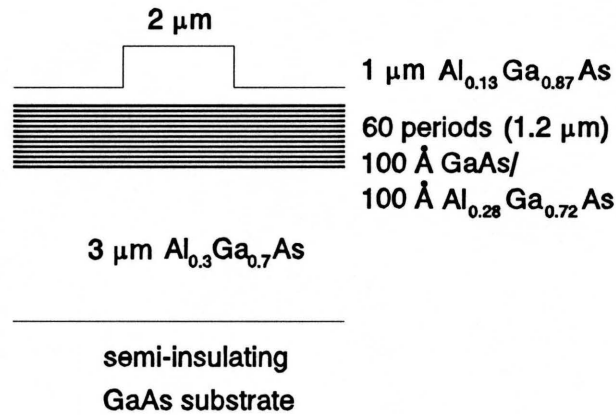


Figure 25. Cross section of single waveguide design.

As discussed previously in chapter 2, a time-bandwidth product of less than 0.3 indicates transform-limited, temporally asymmetric pulses. Since the time-bandwidth product is an absolute minimum for transform-limited pulses, and only asymmetric pulses have a time-bandwidth product of less than 0.3, this combination has the unique property of reducing the product below 0.3. This asymmetry is confirmed by a cross-correlation measurement using the cross-correlator without any sample as shown in Figure 26 (b). The trailing edge of the cross-correlation trace of Figure 26 (b) is noticeably sharper than the rising edge. The two thick lens

systems (microscope objectives) in the specimen beam cause a larger dispersive pulse spread than the thin telescope lenses in the reference beam such that the shorter reference pulses can effectively sample the stretched specimen pulses and detect the asymmetry.

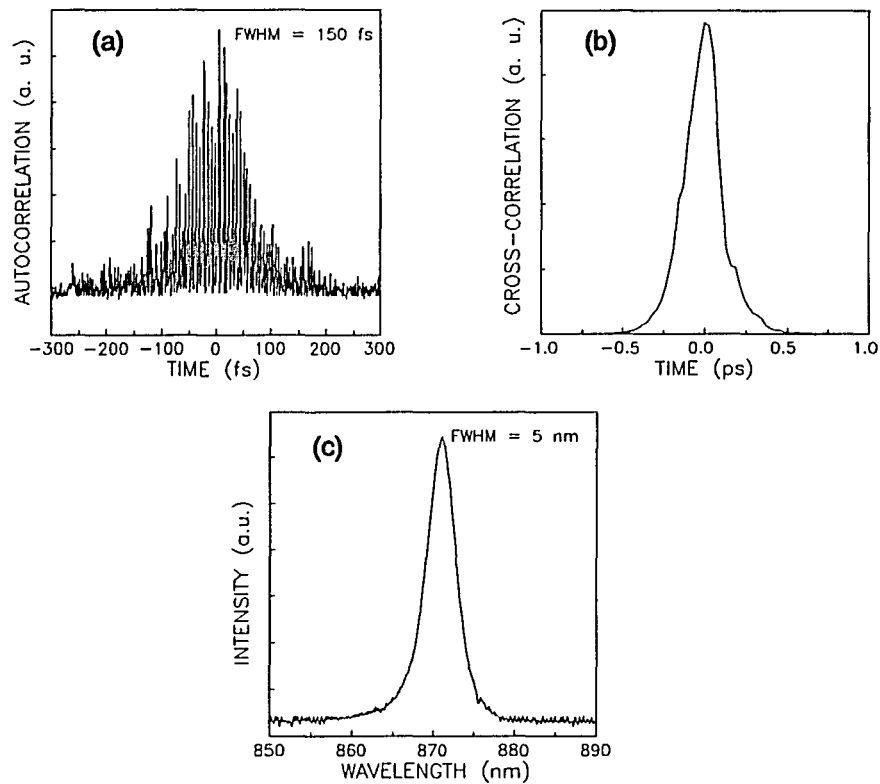


Figure 26. (a) Autocorrelation of the amplified dye laser pulse train. (b) Cross-correlation of the setup without the waveguide. (c) Spectral intensity of the amplified dye laser pulse train.

4.3. Experimental observation of coherent pulse breakup

Figures 27 (a) and 27 (b) show the experimentally measured cross-correlations of the transmitted pulses for both low and high intensity, respectively. Figures 27 (c) and (d) show the corresponding spectral intensities. These results were obtained using a 0.37 mm long waveguide, and peak intensities of 8.5 GW/cm² (Figure 27 (b)) and 0.8 GW/cm² (Figure 27 (a)). The $\Delta t = 4.5$ ps delay observed upon transmission, and which was measured relative to the peak signal without waveguide, is the result of group-velocity delay. Given Δt , the propagation speed v can be calculated using $v = L/t$, where L is the sample length and t is the time of flight through the sample. The time of flight t is the sum of two contributions, the time of flight without sample $t_0 = L/c$ (c is the speed of light in air), and the measured time delay Δt . Then $v = L/(t_0 + \Delta t) = 1/(1/c + \Delta t/L) = 0.21 c$, using $L = 0.37$ mm and $c = 3 \times 10^8$ m/s. In comparison to the input pulse the transmitted low intensity pulse in Figure 27 (a) has a 300 fs FWHM, but does not otherwise show any significant distortion. This temporal spread compared to a 100 fs input pulse can be attributed to linear dispersion mainly in the waveguide coupling optics which stretches the pulse to a 150 fs FWHM even without the waveguide, and the spread inherent in the cross-correlation process using a reference pulse of finite duration. In contrast, pulse breakup is clearly seen in Figure 27 (b) for the high intensity pulse. The main peak of the transmitted pulse still has approximately a 300 fs FWHM, but now a secondary peak appears on the trailing edge of the pulse. Compared to the low intensity spectrum of Figure 27 (c) the high intensity spectral output of Figure 27 (d) features a small shift to the long wavelength side (red-shift) and a shoulder shaped broadening at the long wavelength end of the distribution.

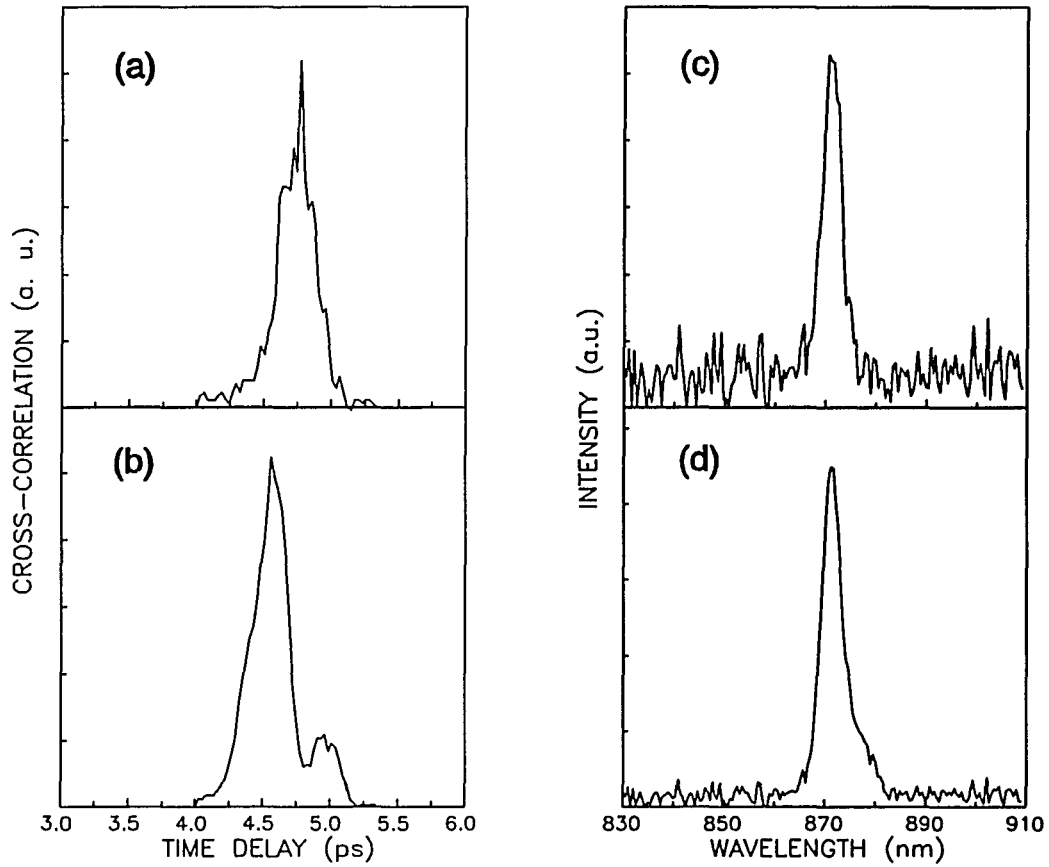


Figure 27. Measured transmitted pulse shapes and spectra of a 0.37 mm long waveguide: (a) is the low intensity (0.8 GW/cm^2) and (b) the high intensity (8.5 GW/cm^2) cross-correlation, (c) and (d) are the spectral intensity distributions that correspond to (a) and (b), respectively.

This series of experiments was also repeated in a slightly longer (0.41 mm) waveguide with transform-limited picosecond pulses of $t_p = 5 \text{ ps}$ FWHM (time-bandwidth product $\Delta\nu \cdot t_p = 0.31$) that were generated by modifying the dye oscillator. A birefringent filter set with a 1:4:16 thickness ratio (0.25 in. thickness of thickest plate) was inserted [Stix et al., 1986] and the saturable absorber jet was turned off. The results are displayed in Figure 28: The cross-

correlation without sample of Figure 28 (a) determines the time delay origin and verifies the input pulse duration. The transmitted pulses through a 0.41 mm long waveguide exhibit no breakup even at 1.1 GW/cm^2 incident peak intensity as shown in Figure 28 (b). Compared to the input spectrum, Figure 28 (c), the transmitted spectral intensity, Figure 28 (d), is slightly broader and shifted to the shorter wavelength side (blue-shift). The input spectrum approaches the resolution of the spectrometer, which explains the pointed curve shape of Figure 28 (c).

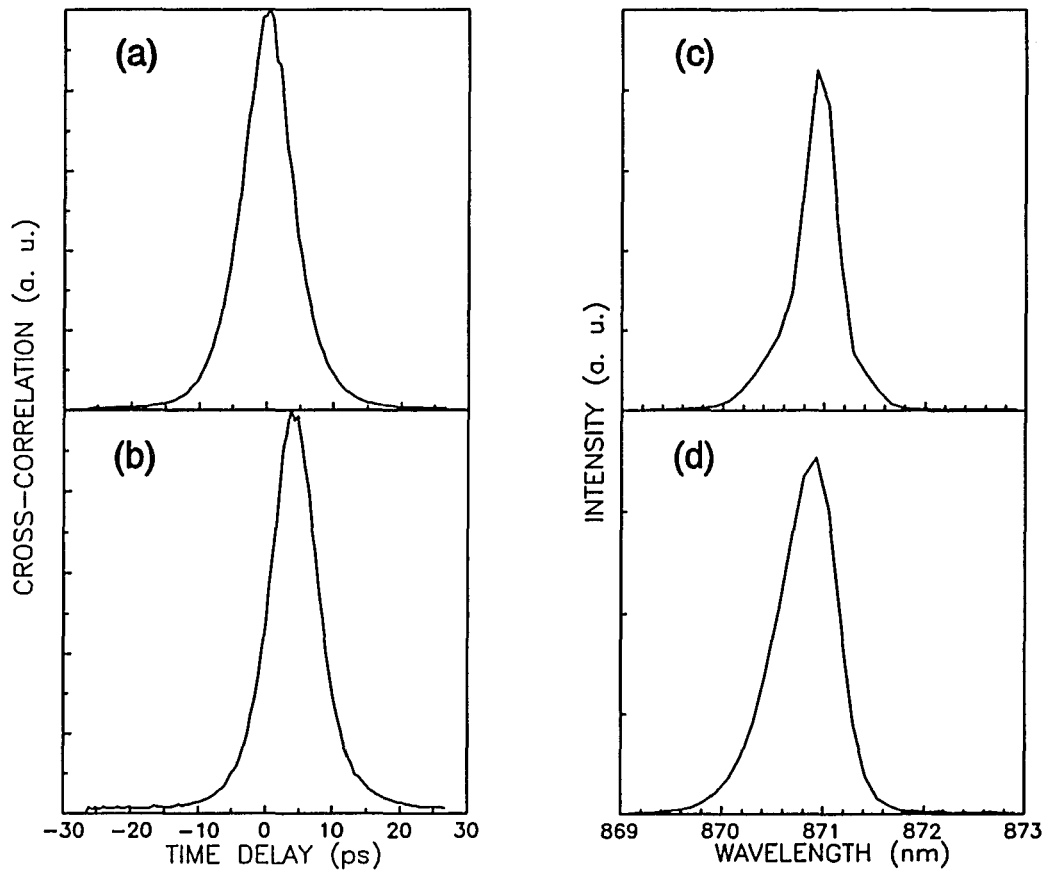


Figure 28. Picosecond pulse cross-correlations of (a) the cross-correlator without waveguide and (b) the output of a 0.41 mm long waveguide at 1.1 GW/cm^2 incident peak intensity. (c) and (d) are the spectral intensity distributions corresponding to (a) and (b), respectively.

Further experimental results obtained with a longer (1.5 mm) waveguide and femtosecond pulses are shown in Figure 29. For the same incident peak intensities as in Figure 27 the transmitted pulse shapes appear very similar to the shorter waveguide output. The low intensity curve, Figure 29 (a), again follows the input pulse shape with no significant distortion, and the high intensity curve, Figure 29 (b), has again acquired a distinct secondary peak on the trailing edge.

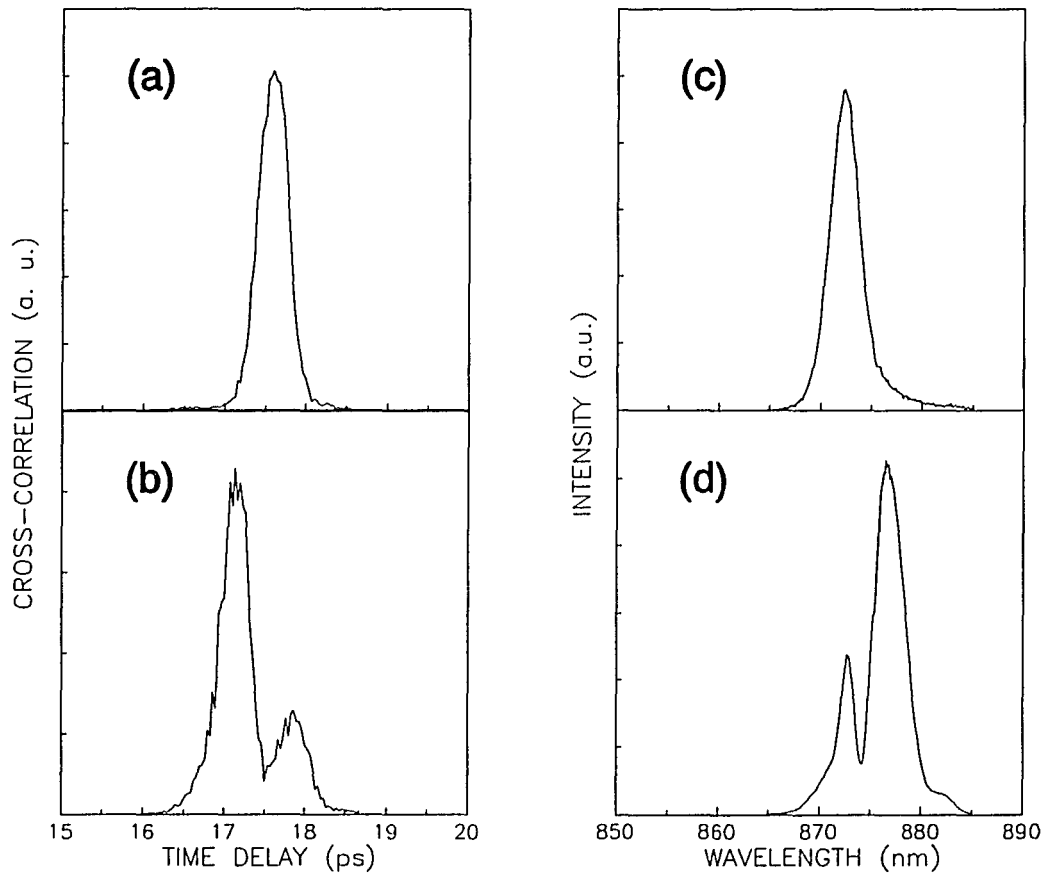


Figure 29. Measured transmitted pulse shapes and spectra of a 1.5 mm long waveguide with the same incident light parameters as Figure 27. (a) and (b) are low and high input intensity cross-correlations, respectively, (c) and (d) are the corresponding spectral intensity distributions.

The increased pulse duration compared to the 0.37 mm waveguide results stems from the effects of group velocity dispersion and light-semiconductor interaction accumulated along an approximately four times longer propagation distance. The spectral shape of the long waveguide output, however, is different compared to the short waveguide output. The low intensity spectrum of Figure 29 (c) already shows a red-shift and broadening at the long wavelength end. The high intensity spectrum of Figure 29 (d) shows strong spectral modulation, or spectral breakup, combined with a large red-shift.

4.4. Propagation-induced escape from adiabatic following

In order to analyze the experimental results the semiconductor Bloch equations [Lindberg and Koch, 1988] are solved self-consistently in combination with Maxwell's equations using fourth order Runge-Kutta numerical integration and fast Fourier transform techniques [see, e.g., Press et al., 1986]. Maxwell's equations for linearly polarized plane waves traveling in the z -direction, which closely approximate the propagating single waveguide mode, yield the wave equation

$$-\frac{\partial^2}{\partial z^2} E(z,t) + \frac{1}{c^2} \frac{\partial^2}{\partial t^2} E(z,t) = -\mu_0 \frac{\partial^2}{\partial t^2} P(z,t) . \quad (25)$$

Here c is the vacuum speed of light and μ_0 is the vacuum magnetic susceptibility. The dispersion in the vicinity of the laser center frequency ω_0 below the semiconductor bandedge is sufficiently smooth so that the propagation constant k is well approximated by an expansion to second order

$$k(\omega) \approx k(\omega_0) + \frac{\partial k}{\partial \omega} (\omega - \omega_0) + \frac{\partial^2 k}{\partial \omega^2} (\omega - \omega_0)^2 . \quad (26)$$

The derivatives, which are to be evaluated at the laser frequency ω_0 , determine the group velocity, $v_g = 1/k' = 1/(\partial k/\partial \omega)$, and the group velocity dispersion, $k_0'' = \partial^2 k/\partial \omega^2$. The total medium polarization can be written as $P(z,t) = P_b(z,t) + P_{nr}(z,t)$. The first part, $P_b(z,t)$, results from the background nonresonant light-matter interaction involving those bands of higher band-index than the conduction band. The second part, $P_{nr}(z,t)$, accounts for the near-resonant interaction between the laser field and conduction and valence bands. For wave packets with several tens of optical cycles and spatial dimensions of several tens of wavelengths the slowly varying envelope approximation is justified. It can symbolically be written as

$$\frac{\partial^2}{\partial z^2} \ll k_0 \frac{\partial}{\partial z} \quad , \quad \frac{\partial^2}{\partial t^2} \ll \omega_0 \frac{\partial}{\partial t} . \quad (27)$$

After inserting the second order dispersion, the polarization separation, and applying the slowly varying envelope approximation, the wave equation becomes [Rudolph and Wilhelmi, 1989]

$$\left(\frac{\partial}{\partial z} + k_0' \frac{\partial}{\partial t} - \frac{i}{2} k_0'' \frac{\partial^2}{\partial t^2} \right) \bar{E}(z,t) = -i \frac{\mu_0}{k_0} \omega_0^2 \bar{P}_{nr}(z,t) , \quad (28)$$

where $k_0 = k(\omega_0)$, $\bar{E}(z,t)$ and $\bar{P}_{nr}(z,t)$ denote the envelopes of the electric field and the near-resonant part of the polarization. Finally the wave equation is transformed into a coordinate system $(\xi, \eta) = (z, t - z/v_g)$ that travels at the group velocity v_g . Then

$$\frac{\partial}{\partial \xi} \bar{E}(\xi, \eta) = -i \frac{\mu_0 \omega_0^2}{2k_0} \bar{P}_{nr}(\xi, \eta) + \frac{i}{2} k_0'' \frac{\partial^2}{\partial \eta^2} \bar{E}(\xi, \eta) . \quad (29)$$

The semiconductor Bloch equations are coupled to the wave equation through the polarization $\bar{P}_{nr}(\xi, \eta)$. In order to keep the numerical effort within reasonable limits \bar{P}_{nr} is derived in the two-band approximation. Exchange effects are neglected since the experiment is performed in the

off-resonance, low-excitation-density regime for which the k-space electron and hole distributions obey $n_{e,k} + n_{h,k} \ll 1$. The semiconductor Bloch equations [Lindberg and Koch, 1988] then take the form

$$\left(\frac{\partial}{\partial \eta} - i \Delta_\lambda + \frac{1}{\tau} \right) \bar{P}_\lambda(\xi, \eta) = -\frac{i}{2\hbar} (1 - 2n_\lambda) d_{cv} \bar{E}(\xi, \eta) , \quad (30)$$

$$\frac{\partial}{\partial \eta} n_\lambda = -\frac{i}{2\hbar} (d_{cv} \bar{P}_\lambda^*(\xi, \eta) \bar{E}(\xi, \eta) - c.c.) . \quad (31)$$

The energy dispersion of the semiconductor material is contained in $\Delta_\lambda = \omega_\lambda - \omega_0$, where λ labels the discrete exciton energy states as well as the continuum states, and ω_0 is the laser center frequency. Here the excitation density in the λ th state is denoted by n_λ and d_{cv} is the dipole transition moment. The phenomenological polarization dephasing time τ is an approximate average over the dephasing times of the different excitations λ , which has provided good agreement between experiment and theory in the case of the optical Stark effect [Lee et al., 1991]. Due to the extremely short pulses used here, the decay of the excitation densities n_λ can be neglected. The desired polarization $\bar{P}_{nr}(\xi, \eta)$ for Equation 29 is obtained as a sum over the relevant polarizations $\bar{P}_\lambda(\xi, \eta)$ from Equations 30 and 31, weighted by the appropriate density $|\Psi_\lambda(0)|^2$, and multiplied by the dipole moment d_{cv} [Haug and Koch, 1990]

$$\bar{P}_{nr}(\xi, \eta) = 2 \sum_\lambda d_{cv}^* |\Psi_\lambda(0)|^2 \bar{P}_\lambda(\xi, \eta) , \quad (32)$$

In the propagation simulations the semiconductor Bloch equations, Equations 30 and 31, including the polarization 32 and the electromagnetic wave equation 29, are solved self-consistently for each small slice of material with the initial values $\bar{P}_\lambda(\xi, \eta = -\infty) = 0$ and $n_\lambda(\xi, \eta = -\infty) = 0$. The electric field resulting from each propagation step serves as the input field for the next. The asymmetry of the pulse entering the waveguide is also included in the model. The

strength of the coherent interaction between light and semiconductor in this two-band model may be quantified by introducing the pulse area A [McCall and Hahn, 1967] with respect to an intraband electron-hole pair state

$$A = \frac{d_{cv}}{\hbar} \left| \int_{-\infty}^{+\infty} \bar{E}(0,t) dt \right| = \int_{-\infty}^{+\infty} \Omega(0,t) dt . \quad (33)$$

The quantity $\Omega(z,t) = d_{cv}\bar{E}(z,t)/\hbar$ is known from atomic physics as the Rabi frequency. The numerical values in the calculation are $d_{cv} = 4.8 \times 10^{-29} \text{ C}\cdot\text{m}$, $\tau = 200 \text{ fs}$, $\hbar\Delta_{1s} = 10 E_R$, where E_R is the bulk exciton Rydberg energy, and $\Delta_{1s} = \omega_{1s} - \omega_0$ is the frequency detuning of the laser from the 1s exciton. The peak Rabi frequency for the high intensity (8.5 GW/cm^2 peak intensity) femtosecond input is $\Omega_0 = 10^{14} \text{ Hz}$, which corresponds to a pulse of area $A = 7.5\pi$, under the assumption that the input pulse has slightly spread to about 150 fs FWHM through the input coupling lens system. The group refractive index, which is defined as the ratio of the vacuum speed of light to the group velocity, $n^* = c/v_g$, is determined in our experiment by replacing v_g with the propagation speed v , yielding $n^* = c/v = 4.76$. This value is consistent with a group index measurement in GaAs double heterostructure lasers at similar detuning from the bandedge [van der Ziel and Logan, 1983]. The amounts of group velocity dispersion assumed to simulate the semiconductor medium and the output coupling lens system together spread the incident pulse by a factor of 1.33 under linear propagation through the short (0.37 mm) waveguide.

Figure 30, corresponding to the experimental results in Figure 27, shows the calculated cross-correlations and spectral intensity distributions of the transmitted pulses obtained by numerically integrating the coupled semiconductor Maxwell-Bloch equations, Equations 29-32 using the above parameters. Very good agreement between theoretical cross-correlations, Figures

30 (a) and (b), and experimental cross-correlations, Figures 27 (a) and (b), is obtained with pulse breakup clearly evident only for the high intensity, large area (7.5π) pulses in Figures 27 (b) and 30 (b).

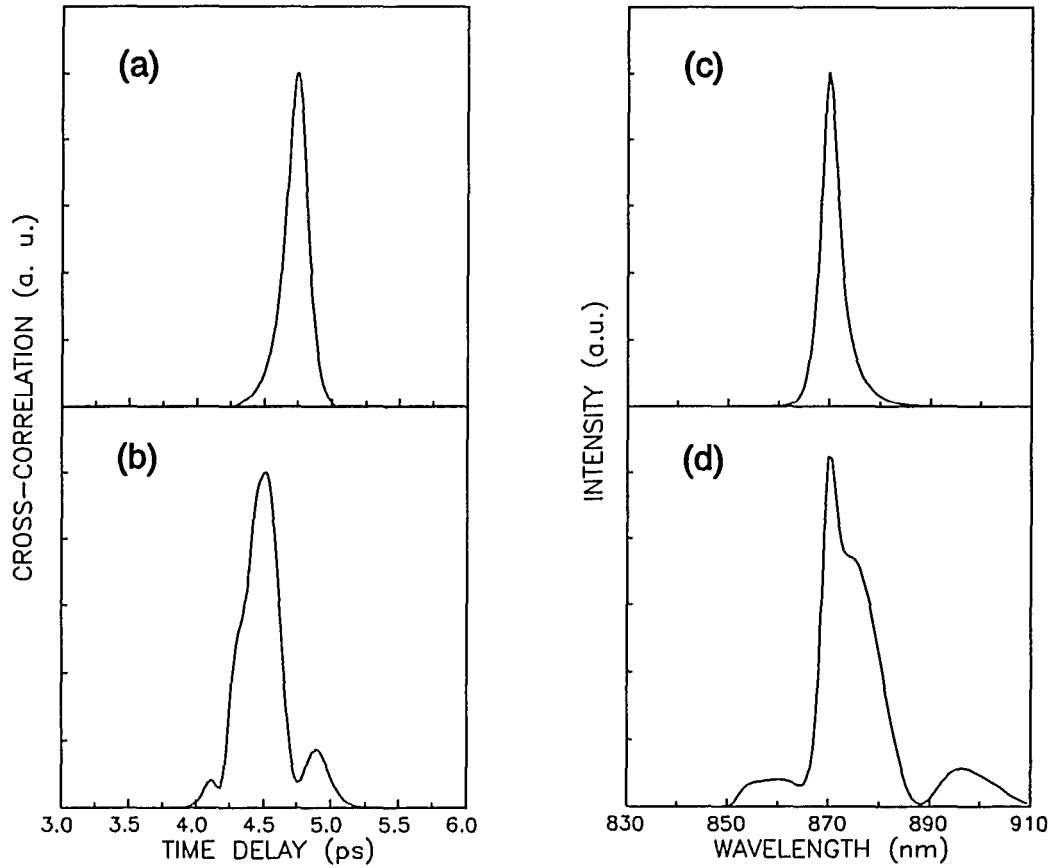


Figure 30. Theoretical pulse shape and spectral results for the 0.37 mm long waveguide: (a) is the low intensity, small area (2π) and (b) the high intensity, large area (7.5π) cross-correlation, (c) and (d) are the spectral intensity distributions that correspond to (a) and (b), respectively.

The labels "high intensity" and "low intensity" are used here in a relative sense similar to the digital "high" and "low" states. "Low intensity" does not imply a regime of negligible light-semiconductor interaction. The low intensity regime is here defined as pulse propagation that satisfies the adiabatic following conditions at every point within the waveguide.

The theoretical spectra, Figures 30 (c) and (d), and the experimental data, Figures 27 (c) and (d), agree qualitatively. The low intensity, small area curve, Figure 30 (c), undergoes no spectral modulation while the high intensity, large area case, depicted in Figure 30 (d), confirms the experimentally observed features, namely the red-shift and the broadening toward the long wavelength side.

The simulations of the 1.5 mm waveguide propagation, shown in Figure 31, qualitatively reproduce the dominant experimentally measured features of Figure 29. These are the following: no significant temporal distortion in the low intensity, small area cross-correlations of Figure 31 (a), red-shift and long wavelength shoulder development in the low intensity, small area spectrum of Figure 31 (c), and finally, temporal, as well as spectral breakup accompanied by a large red-shift for the high intensity, large area input pulse cross-correlation and spectrum of Figures 31 (b) and (d), respectively. For distances longer than about $z = \xi = 300 \mu\text{m}$ the propagation is controlled by the linear properties of the medium, since the pulse amplitude has decayed significantly due to absorption. In this regime the difference in absorption between the short wavelength side of the transmitted light (closer to the bandedge) and the long wavelength side (further away from the bandedge) causes a red-shift of the spectrum. The larger red-shift for the longer sample is consistent with this argument.

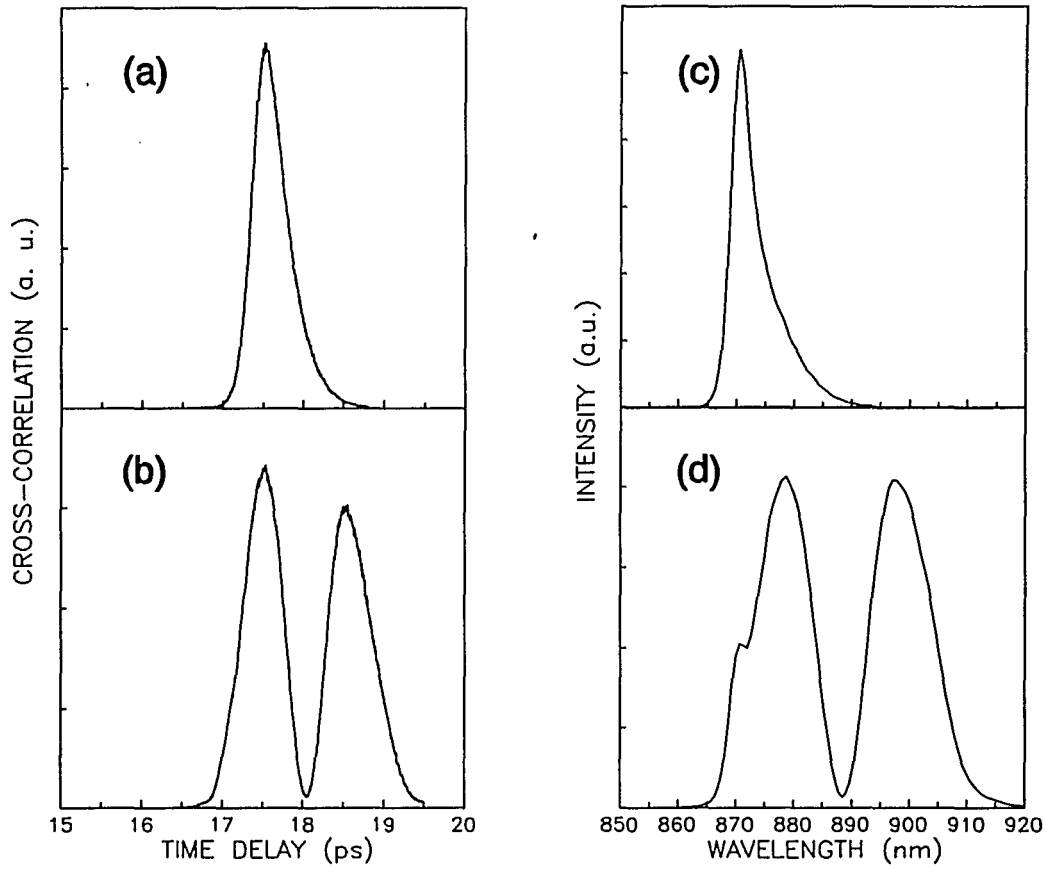


Figure 31. Theoretical pulse shapes and spectral results for the 1.5 mm long waveguide with the same incident light parameters as Figure 30. (a) and (b) are low and high intensity cross-correlations, respectively, (c) and (d) are the corresponding spectral intensity distributions.

The limitations of the theoretical simulations become apparent in the merely qualitative agreement of the calculated spectra of Figures 30 (d) and 31 (d) and the calculated cross-correlation of Figure 31 (b) with the experimental results of Figures 27 (d), 29 (d) and (b), respectively. The predominant restrictions of the theory are these:

Firstly, the excitonic resonance is approximated by a homogeneously broadened Lorentzian absorption curve. This does not conform with the experimentally determined Gaussian shape [Chemla et al., 1984]. A Lorentzian line shape over-estimates the absorption far away from line center. It also misrepresents the variation of absorption with wavelength, which decreases the accuracy of the longer propagation distance simulations. Haug and Koch [Haug and Koch, 1990] point out that a better theoretical model would incorporate a light frequency dependent damping parameter in the Lorentzian absorption. In this case, however, the computation time would escalate to impractical values.

Secondly, the dephasing times of all band states, including the excitonic states, are replaced by the single average value $\tau = 200$ fs. This approximation has yielded good results in the case of the optical Stark effect. However, pulse propagation calculations that attempt to reproduce the detailed temporal and spectral pulse shapes are more sensitive to an inaccurate, average dephasing time superposition of the induced coherent polarizations.

Thirdly, the simulations disregard waveguiding effects. Wavelength dependent loss due to the waveguide design causes an estimated intensity loss for a 1 mm long waveguide of about 40 % in the spectral band of interest. This loss reduces the peak intensity of the propagating pulse, adding to the effect of intrinsic absorption in the semiconductor medium. This further decreases the nonlinear interaction at longer propagation distances. The wavelength dependent guiding loss contributes to the dispersive parameters of the problem that govern pulse spreading and propagation delay. The main feature of the simulated cross-correlations, i. e. pulse breakup for large area pulses, has, however, proven remarkably insensitive to the magnitude of the group velocity dispersion constant. The transverse (x,y) dimensions are not included in our model, neglecting the possibility of spatial pulse breakup and coupling into higher order transverse modes.

To obtain a deeper physical understanding of what is responsible for the pulse breakup an extensive series of diagnostic tests involving the calculated excitation density $N = 2 \sum |\psi_\lambda(0)|^2 n_\lambda$ and the pulse shape at different locations ξ within the waveguide has been performed. In Figure 32 at $z = \xi = 0 \mu\text{m}$ the excitation density N is seen to closely follow the input intensity with no oscillations. As discussed in chapter 3.5. this is consistent with the adiabatic following hypothesis [Allen and Eberly 1975] and the optical Stark effect, though a residual density remains after the pulse due to the finite polarization dephasing time. Thus the pulse breakup can not be simply ascribed to off-resonance Rabi-oscillations in the excitation density as found in self-induced transparency: The effective Rabi-frequency can only decrease with propagation distance since the field amplitude is decaying, excluding the possibility of Rabi-oscillations downstream. Also note that, in comparison to the work of Grischkowsky et al. in Rb vapor [Grischkowsky et al., 1973], the temporal pulse profile does not show a significant increase in the slope of its leading edge, ruling out pulse-steepening as a possible explanation. However, the calculations of Figures 32 (a) and (b) show at $z = \xi = 120 \mu\text{m}$ that oscillations in the excitation density have already fully unfolded while the light intensity merely shows a small shoulder. The origin of the pulse breakup can therefore be attributed to the preceding excitation density oscillations. To make this clearer, if the effects of group velocity dispersion are neglected in Equation 29, the combined Equations 29-32 yield the exact result

$$\frac{\partial}{\partial \xi} |\bar{E}(\xi, \eta)|^2 = - \frac{\hbar \mu_0 \omega_0^2}{k_0} \frac{\partial N}{\partial \eta} . \quad (34)$$

So temporal oscillations in N are converted to temporal oscillations in the pulse intensity profile $|\bar{E}(\xi, \eta)|^2$ through propagation, $|\bar{E}(\xi + d\xi, \eta)|^2 - |\bar{E}(\xi, \eta)|^2 \propto \partial N / \partial \eta$. This approximate result gains significance in light of the fact that the calculations continue to produce pulse breakup even without group velocity dispersion ($k_0'' = 0$).

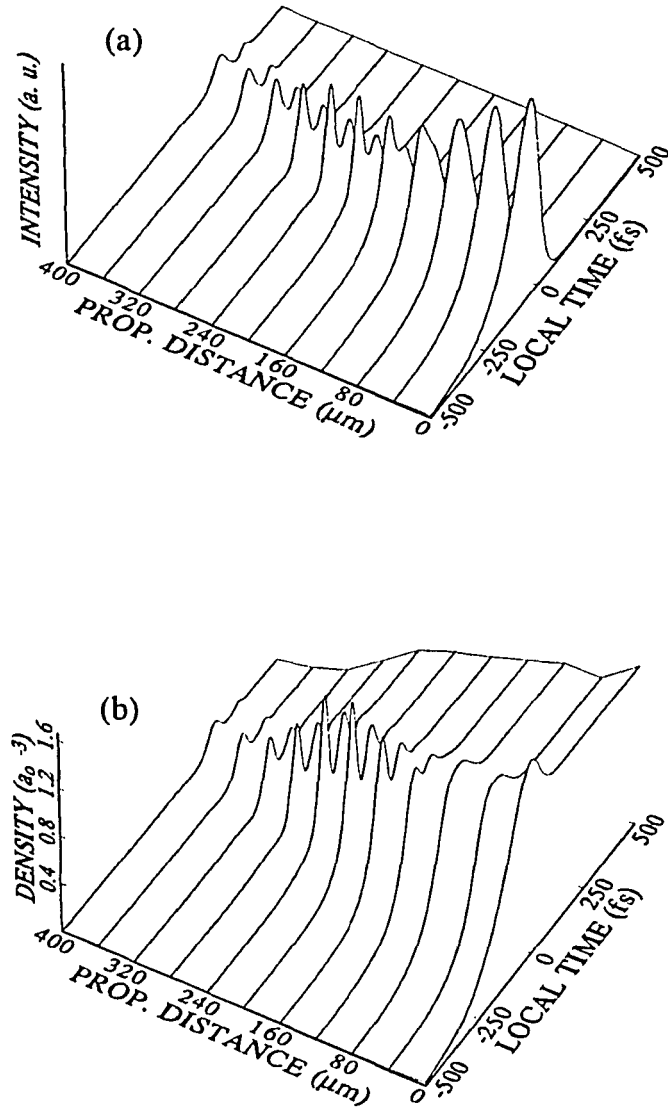


Figure 32. (a) Calculated pulse intensity and (b) total carrier density profiles as a function of propagation distance. Local time refers to the coordinate η of the moving frame that travels with group-velocity v_g . a_0 is the exciton Bohr radius.

The oscillations in the excitation density that trigger the pulse breakup are a direct consequence of the coherent nature of the light-matter interaction in this case. To see this, one first formally integrates Equation 30 to obtain

$$\bar{P}_\lambda(\xi, \eta) = -\frac{id_{cv}}{2\hbar} \int_{-\infty}^{\eta} (1 - 2n_\lambda(\xi, \eta')) \bar{E}(\xi, \eta') e^{[i(\omega_\lambda - \omega_0) - 1/\tau](\eta - \eta')} d\eta' . \quad (35)$$

The coherent character of the interaction is implicit in the fact that the polarization depends on the prior temporal history of the electric field. Inserting Equation 35 into 31 we see that the excitation density n_λ is driven by interference terms of the form $\bar{E}(\xi, \eta)\bar{E}^*(\xi, \eta')$, between the field at retarded time η and earlier times η' . The dominant contributions to these terms come from times obeying $\eta - \eta' < \tau$. For $t_p \gg \tau$, on the other hand, the exponent $\exp(-(\eta - \eta')/\tau)$ becomes strongly damped; the polarization then adiabatically follows the field (time history erased), and the interference terms vanish [Allen and Eberly, 1975]. Note that this is in perfect accord with the experimental and numerical results for long pulses ($t_p = 5\text{ps} \gg \tau = 200\text{fs}$) for which pulse breakup was absent. If in the coherent case ($t_p \ll \tau$) the propagating field is sufficiently frequency chirped by self-phase modulation, i. e. the instantaneous frequency of the pulse $\omega(t) = d\phi/dt$ develops a dominant term that is linear in time t , then the phase ϕ of the electric field can vary rapidly enough to escape from the adiabatic following regime. Self-phase modulation refers to the phenomenon in which an intense light field induces an appreciable refractive index change. The medium then reacts back, imposing a phase modulation on the incident beam [see Shen and Yang, 1989, and references therein]. Note that not only rapid electric field envelope changes, but also rapid electric field phase changes can violate the adiabatic following approximation. The resulting interference terms that drive oscillations in the excitation density then, in turn, cause pulse breakup.

In order to test this mechanism for pulse breakup consider the numerically calculated field at $\xi = 120 \mu\text{m}$, which can be written in terms of its real amplitude \mathcal{E} and phase ϕ , $\bar{E}(\xi = 120 \mu\text{m}, \eta) = \mathcal{E}(\eta)\exp(i\phi(\eta))$. As seen in Figure 33, while the amplitude $\mathcal{E}(\eta)$ merely shows a small modulation (dashed curve in Figure 33 (a)) the density N (solid curve in Figure 33 (b)) is already oscillating, driven by the large frequency chirp of the instantaneous light frequency, $\Delta\omega(\eta) = -\partial\phi/\partial\eta$. A fit of the phase curve to the function $\phi(\eta) \approx \phi_1\eta + \phi_2\eta^2$ around $\eta = 0$, with frequency chirping being represented by the second term, reveals that the chirp term really is the most important. Figure 33 (b) shows the solution of the semiconductor Bloch equations at $\xi = 120 \mu\text{m}$ for the cases (I) exact numerical solution, (II) $\phi(\eta) = \phi_1\eta$, and (III) $\phi(\eta) = \phi_1\eta + \phi_2\eta^2$. It is clear that the approximate simulation including frequency chirping (curve III) is in much better agreement with the exact numerical solution, thus demonstrating that frequency chirping due to self-phase modulation indeed results in interference terms that drive the excitation density oscillations.

In a Bloch-vector representation one can describe the light-semiconductor interaction at $\xi = 0$ by adiabatic following, i.e., the rate of change of \bar{E} ($\approx 1/100$ fs) is slow compared with the precession frequency $(\Omega^2 + \Delta_{\text{is}}^2)^{1/2}$, and the Bloch-vector $\bar{\mathbf{p}}$ follows the torque vector. But by $\xi = 120 \mu\text{m}$, $\partial\phi/\partial\eta$ instantaneously reaches $\Delta_{\text{is}}/2$. This violates the adiabatic following criterion since $\partial\bar{E}/\partial\eta \approx i \partial\phi/\partial\eta \bar{E}$, when $\partial\phi/\partial\eta$ is large. This is true according to the definition of Allen and Eberly used so far [Allen and Eberly, 1975], but adiabatic following is also violated in a frame rotating at $\omega_0 + \partial\phi/\partial t$ as in Grischkowsky's definition [Grischkowsky, 1970]. In Bloch-vector jargon the effective field moves too fast for $\bar{\mathbf{p}}$ to follow; with a component of the effective field perpendicular to $\bar{\mathbf{p}}$, $\bar{\mathbf{p}}$ is rotated, giving oscillations in the carrier density N .

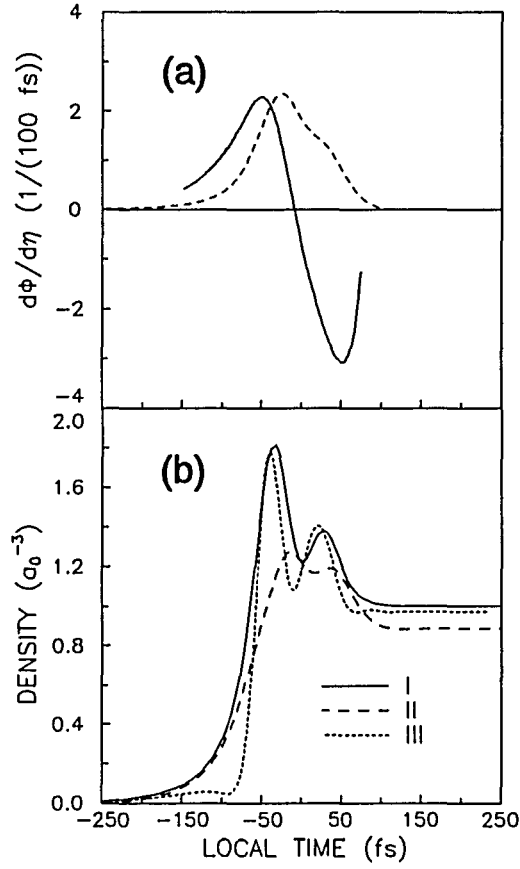


Figure 33. (a) Calculated frequency chirp $d\phi/d\eta$ (solid line) at $\xi = 120 \mu\text{m}$. The pulse intensity (dashed line) is plotted for reference. (b) Temporal profiles of the carrier density N at $\xi = 120 \mu\text{m}$ resulting from solving the semiconductor Bloch equations with the exact numerical phase solution $\phi(\eta)$ (I, solid line), a first order fit $\phi(\eta) = \phi_1\eta$ (II, long dashed line), and a second order fit $\phi(\eta) = \phi_1\eta + \phi_2\eta^2$ (III, short dashed line).

4.5. Conclusion

Below-resonance, coherent pulse breakup has been observed for the first time in a room temperature semiconductor waveguide. Detailed numerical simulations of pulse propagation

using the coupled semiconductor Maxwell-Bloch equations reproduce these results well and yield pulse breakup even in the absence of group velocity dispersion revealing the coherent nature of the effect. The interaction between a light pulse with a duration less than the polarization dephasing time of the material is shown to accumulate enough self-phase modulation induced chirp during propagation in order to escape from the initial adiabatic following regime, thus the name of section 4.4., propagation-induced escape from adiabatic following. This coherent effect is distinctly different from self-induced transparency, because it does not involve Rabi-oscillations at the start of propagation, from temporal solitons, because it does not require group velocity dispersion, and from self-steepening, because no steepening of the leading edge of the pulse is observed. However, it should be ubiquitous under off-resonance pulse propagation with a pulse duration less than the polarization dephasing time.

CHAPTER 5

DIRECTIONAL COUPLER COHERENT PULSE PROPAGATION AND FUTURE EXPERIMENTS

5.1. Preliminary coherent pulse propagation results in directional couplers

The measurements of the previous chapter have been repeated with a 0.88 mm long directional coupler of the same design that is shown in chapter 3, page 47, Figure 17. Again low intensity and high intensity transmitted pulse shapes and spectral shapes have been recorded using the cross-correlator setup of chapter 4, page 62, Figure 24. The incident pulse cross-correlation and spectral distribution were inspected before the experiment, ensuring that they are transform-limited as shown in chapter 4, page 64, Figure 26. The input peak intensities in this single beam experiment were chosen above (high intensity, 3.5 GW/cm^2) and below (low intensity, 0.85 GW/cm^2) the switching peak intensity of 2 GW/cm^2 that had been determined in chapter 3, page 51, Figure 20. The time-integrated spatial intensity distributions of the directional coupler output ports are shown in Figure 34 for the above peak intensities. The pulses are initially injected into channel 2. The difference between the low intensity (Figure 34 (a)) and the high intensity (Figure 34 (b)) profiles demonstrates switching from a situation, where most of the light exits channel 1, to a situation, where most of it leaves channel 2. For all Figures in this section the labels "1" and "2" denote channel 1 and channel 2, respectively.

Figures 35 (a) and (b) depict high intensity and low intensity cross-correlations of both channels, respectively, corresponding to Figures 34 (a) and (b). Surprisingly, the low intensity

curves (Figure 35 (a)), which look almost identical for both channels, exhibit pulse breakup, although pulses of the same peak intensity have not shown any coherent pulse breakup in the single waveguide experiments of chapter 4 (see Figures 27, page 66, and 29, page 68). This clearly reveals that the evanescent coupling between the waveguides modifies the coherent interaction between light and semiconductor in each waveguide. The detailed physical mechanisms involved require further research. A theoretical description of this experiment will have to include the transverse (x,y) coordinates, because the coupling between the waveguides is itself a transverse effect. The propagation delay difference for the two channels in Figure 35 (a) suggests different effective propagation distances. The light that emerges from channel 1 had to couple over into the other waveguide, while the light emerging from channel 2 remained in the input waveguide.

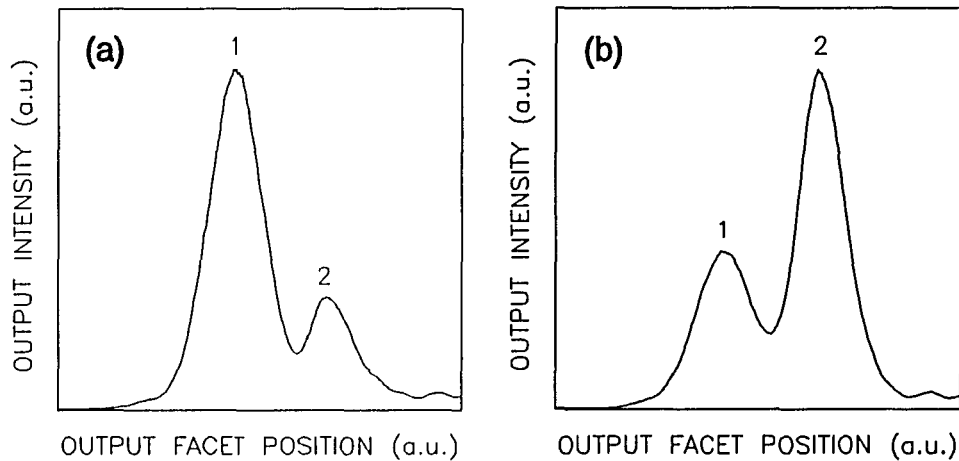


Figure 34. (a) Low intensity (0.85 GW/cm²) and (b) high intensity (3.5 GW/cm²) time-integrated intensity distribution between the two channels of a 0.88 mm long directional coupler for single pulses injected into channel 2.

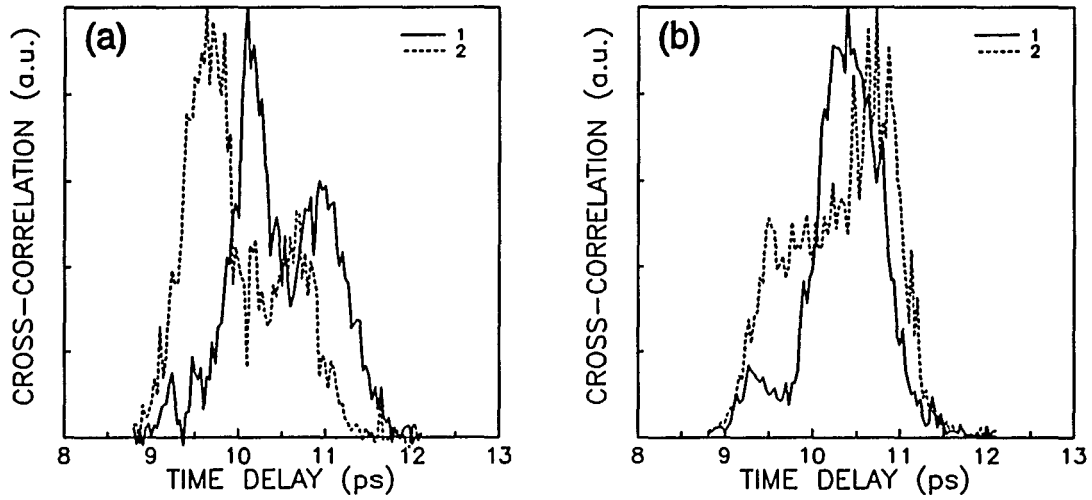


Figure 35. (a) Low intensity cross-correlations corresponding to Figure 34 (a), (b) high intensity cross-correlations corresponding to Figure 34 (b); solid curves: channel 1, dashed curves: channel 2.

The high intensity cross-correlations of Figure 35 (b) also show pulse breakup, but differ in shape from the low intensity curves of Figure 35 (a) and from each other. In this case most of the light is assumed to stay in the input waveguide, channel 2, under the influence of strong nonlinear perturbation. The pulses in both waveguides break up into a smaller leading portion followed by a larger trailing component.

The spectral intensities that correspond to Figures 34 and 35 are depicted in Figure 36, Figure 36 (a) showing the low intensity case, and Figure 36 (b) showing the high intensity case.

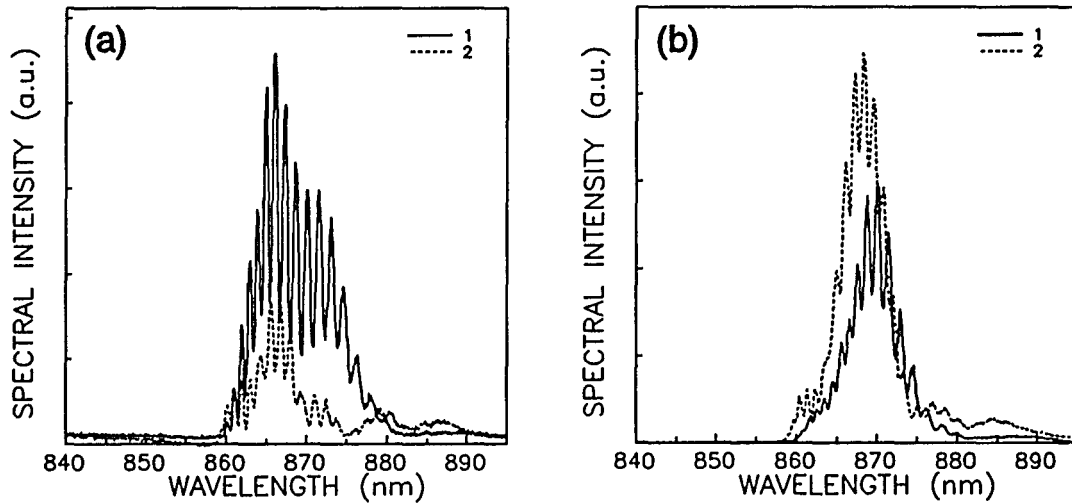


Figure 36. Transmitted spectral intensities of the 0.88 mm directional coupler, corresponding to Figures 34 and 35; (a) low intensity, (b) high intensity; solid lines: channel 1, dashed lines: channel 2.

The low intensity curves (Figure 36 (a)) show large spectral broadening towards the long wavelength side, particularly the channel 1 output, which carries most of the light in this case. The high intensity curves (Figure 36 (b)) exhibit less spectral broadening toward the long wavelength side, but the peak spectral emission of the two channels occurs at different

wavelengths. All spectra appear to be strongly modulated in a common sinusoidal way. At this time the described temporal and spectral features are not well explained.

5.2. Suggestions for Future Experiments

It would be helpful to repeat the measurements of section 5.1. with pulse durations that are much longer than the polarization dephasing time of the medium ($t_p \gg 200$ fs). If the pulse breakup in the directional coupler persists under these circumstances, the breakup is, at least in part, due to incoherent effects. If not, the coherent interaction is identified as the reason for the breakup. Once the properties and roles of the involved coherent and incoherent processes are recognized, strategies for breakup prevention can be devised. In the case of a Kerr nonlinearity, as described in chapter 3, page 44, the breakup would be caused by the intensity dependence of the induced phase change. The peak of the pump pulse would generate the largest phase change and switch only the central portion of the probe, leaving its leading and trailing edges behind. This could be overcome by using a pump pulse of much longer duration than the probe.

As indicated in the conclusion of chapter 3, further in-depth studies are needed to explore the possibility of supplying the directional coupler with gain. The first objective, regarding practical device applications, would be to increase the throughput to at least the 50 % level. The optical properties of the semiconductor medium completely change during the transition from absorption to gain. This could give rise to new, interesting, and useful effects, e. g. soliton-like pulse propagation. One possible scenario for a soliton-like behavior is found, when the pulse is spectrally centered at the crossing point between gain and absorption [Kesler and Ippen, 1987].

In this case one half of the pulse experiences amplification, while the other half experiences absorption, facilitating unattenuated passage through the medium.

The arrival of the tunable femtosecond Ti:sapphire laser provides the opportunity to perform these measurements as a function of wavelength. Taking cross-correlations for different wavelengths the dependence of propagation delay on frequency detuning could be determined. This method produces very accurate data for the group refractive index n^* .

These two directions of further experimental research could be well complemented by theoretical studies that extend the existing model based on the coupled semiconductor Maxwell-Bloch equations by incorporating evanescent coupling between waveguides and gain.

Appendix: List of Publications

- P. A. Harten, A. Knorr, J. P. Sokoloff, F. Brown de Colstoun, S. G. Lee, R. Jin, E. M. Wright, G. Khitrova, H. M. Gibbs, S. W. Koch, and N. Peyghambarian, "Propagation-induced escape from adiabatic following in a semiconductor", *Phys. Rev. Lett.* **69**, 852 (1992).
- P. A. Harten, S. G. Lee, J. P. Sokoloff, J. R. Salcedo, and N. Peyghambarian, "Noise in a Dual Dye Jet Hybridly Mode-Locked Near Infrared Femtosecond Laser", *Opt. Commun.* **91**, 465 (1992).
- P. A. Harten, A. Knorr, J. P. Sokoloff, F. Brown de Colstoun, S. G. Lee, R. Jin, E. M. Wright, G. Khitrova, H. M. Gibbs, S. W. Koch, and N. Peyghambarian, "Coherent pulse propagation in a semiconductor waveguide," *International Conference on Quantum Electronics Technical Digest Series* **9**, 386 (1992).
- P. A. Harten, A. Knorr, J. P. Sokoloff, F. Brown de Colstoun, S. G. Lee, R. Jin, E. M. Wright, G. Khitrova, H. M. Gibbs, S. W. Koch, and N. Peyghambarian, "Observation and theoretical verification of coherent pulse breakup in gallium arsenide quantum well waveguides", *Digest of Ultrafast Phenomena VIII*, 330 (E.N.S.T.A., Paris 1992).
- P. A. Harten, A. Knorr, J. P. Sokoloff, F. Brown de Colstoun, S. G. Lee, R. Jin, E. M. Wright, G. Khitrova, H. M. Gibbs, S. W. Koch, and N. Peyghambarian, "Optical switching and propagation effects in nonlinear GaAs MQW waveguides", *Proc. SPIE* **1626**, 168 (1992).
- N. Peyghambarian, P. A. Harten, A. Knorr, J. P. Sokoloff, F. Brown de Colstoun, S. G. Lee, R. Jin, E. M. Wright, G. Khitrova, H. M. Gibbs, and S. W. Koch, "Coherent pulse breakup in femtosecond pulse propagation in semiconductors," to be published in *phys. stat. sol. (b)* **173** (1992).
- N. Peyghambarian, R. Binder, C. L. Chuang, F. Brown de Colstoun, B. Fluegel, H. M. Gibbs, P. A. Harten, R. Jin, G. Khitrova, S. W. Koch, S. G. Lee, K. Meissner, and J. P. Sokoloff, "Femtosecond Nonlinear Optics of Semiconductor Quantum Wells", *Proceedings of the National Colloquium "Recent Advances in the Uses of Light in Physics, Chemistry, Engineering, and Medicine"*, City College of New York (1991).
- C. L. Chuang, R. Jin, Jiajin Xu, P. A. Harten, G. Khitrova, H. M. Gibbs, S. G. Lee, J. P. Sokoloff, N. Peyghambarian, R. Fu, C. S. Hong, "GaAs/AlGaAs Multiple Quantum Well Nonlinear Optical Directional Coupler", accepted for publication in *Journal of Nonlinear Optics* (1991).
- S. G. Lee, P. A. Harten, J. P. Sokoloff, R. Jin, B. Fluegel, K. E. Meissner, C. L. Chuang, R. Binder, S. W. Koch, G. Khitrova, H. M. Gibbs, N. Peyghambarian, J. N. Polky, G. A. Pubanz, "Femtosecond Excitonic Bleaching Recovery in the Optical Stark Effect of

- GaAs-AlGaAs Multiple Quantum Wells and Directional Couplers", *Phys. Rev. B*, **43**, 1719 (1991).
- P. A. Harten, R. Jin, J. P. Sokoloff, C. L. Chuang, S. G. Lee, M. Warren, H. M. Gibbs, N. Peyghambarian, J. N. Polky, G. A. Pubanz, "Subpicosecond All-Optical Modulation in a GaAs/AlGaAs Directional Coupler", *Conference on Lasers and Electro-Optics Technical Digest Series 7*, 482 (1990).
- J. P. Sokoloff, S. G. Lee, R. Jin, P. A. Harten, R. Binder, S. W. Koch, H. M. Gibbs, N. Peyghambarian, "Femtosecond Recovery of Exciton Bleaching in the Optical Stark Effect", *Conference on Lasers and Electro-Optics Technical Digest Series 7*, 176 (1990)..
- C. L. Chuang, R. Jin, M. Warren, H. M. Gibbs, J. P. Sokoloff, P. A. Harten, N. Peyghambarian, J. N. Polky, G. A. Pubanz, "Fabrication and Performance of GaAs - MQW Nonlinear Directional Coupler", *Proc. SPIE* **1216**, 13 (1990).
- H. M. Gibbs, R. Jin, P. A. Harten, J. P. Sokoloff, C. L. Chuang, S. G. Lee, M. Warren, N. Peyghambarian, J. N. Polky, and G. A. Pubanz, "Picosecond and Subpicosecond Switching and Modulation in GaAs/AlGaAs Nonlinear Directional Couplers", paper WH6, *OSA Conference on Integrated Photonics Research* (1990).
- R. Jin, J. P. Sokoloff, P. A. Harten, C. L. Chuang, S. G. Lee, M. Warren, H. M. Gibbs, N. Peyghambarian, J. N. Polky, G. A. Pubanz, "Ultrafast Modulation with Subpicosecond Recovery Time in a GaAs/AlGaAs Nonlinear Directional Coupler", *Appl. Phys. Lett.*, **56**, 993 (1990).
- J. P. Sokoloff, P. A. Harten, R. Jin, C. L. Chuang, M. Warren, H. M. Gibbs, S. G. Lee, and N. Peyghambarian, "Subpicosecond All-Optical Modulation Using the Optical Stark Effect in a Nonlinear Directional Coupler", *Proc. SPIE* **1138**, 13 (1989).
- R. Jin, C. L. Chuang, H. M. Gibbs, M. Warren, J. Sokoloff, P. Harten, N. Peyghambarian, J. N. Polky, G. A. Pubanz, paper ME1, *OSA 1989 Technical Digest Series* **11**, 12 (1989).

References

- L. Allen and J. H. Eberly, *"Optical Resonance and Two-Level Atoms"* (Wiley, New York, 1975).
- C. P. Ausschnitt, R. K. Jain, and J. P. Heritage, "Cavity length detuning characteristics of the synchronously mode-locked cw dye laser," *IEEE J. Quant. Electron.* **15**, 912 (1979).
- P. C. Becker, H. L. Fragnito, C. H. Brito Cruz, R. L. Fork, J. E. Cunningham, J. E. Henry, and C. V. Shank, "Femtosecond photon echoes from band-to-band transitions in GaAs," *Phys. Rev. Lett.* **61**, 1647 (1988).
- R. Binder, S. W. Koch, M. Lindberg, N. Peyghambarian, and W. Schäfer, "Ultrafast adiabatic following in semiconductors," *Phys. Rev. Lett.* **65**, 899 (1990a).
- R. Binder, M. Lindberg, S. W. Koch, and N. Peyghambarian, "Theory of femtosecond transient exciton bleaching and recovery in the optical Stark effect," *Proc. SPIE* **1216**, 74 (1990b).
- R. Binder, S. W. Koch, M. Lindberg, W. Schäfer, and F. Jahnke, "Transient many-body effects in the semiconductor optical Stark effect," *Phys. Rev. B* **43**, 6520 (1991).
- Zs. Bor and B. Rácz, "Group velocity dispersion in prisms and its application to pulse compression and travelling-wave excitation," *Opt. Commun.* **54**, 165 (1985).
- L. W. Casperson, "Coherence effects in synchronously pumped mode-locked dye lasers," *J. Appl. Phys.* **54**, 2198 (1983).
- D. S. Chemla, D. A. B. Miller, P. W. Smith, A. C. Gossard, and W. Wiegman, "Room temperature excitonic absorption and refraction in GaAs/AlGaAs multiple quantum well structures," *IEEE J. Quant. Electron.* **QE-20**, 265 (1984).
- C. L. Chuang, Ph. D. Dissertation, University of Arizona, Optical Sciences Center, Tucson (1991).
- M. D. Dawson, T. F. Boggess, D. W. Garvey, and A. L. Smirl, "A hybridly mode-locked cw dye laser with Brewster prisms," *Opt. Commun.* **60**, 79 (1986).
- M. D. Dawson, T. F. Boggess, and A. L. Smirl, "Femtosecond synchronously pumped pyridine dye lasers," *Opt. Lett.* **12**, 254 (1987).
- M. D. Dawson, D. Maxson, T. F. Boggess, and A. L. Smirl, "Cavity-length detuning effects and stability of a synchronously pumped femtosecond linear dye laser," *Opt. Lett.* **13**, 126 (1988).

- J.-C. M. Diels, J. J. Fontaine, I. C. McMichael, and F. Simoni, "Control and measurement of ultrashort pulse shapes (in amplitude and phase) with femtosecond accuracy," *Appl. Opt.* **24**, 1270 (1985).
- J.-C. M. Diels, "Femtosecond dye lasers", in *"Dye Laser Principles With Applications,"* F. J. Duarte and L. W. Hillman, Eds. (Academic Press, San Diego, 1990, and references therein).
- J. Dobler, H. H. Schulz, and W. Zinth, "Generation of femtosecond light pulses in the near infrared around $\lambda = 850$ nm," *Opt. Commun.* **57**, 407 (1986).
- N. Finlayson, W. C. Banyai, E. M. Wright, C. T. Seaton, G. I. Stegeman, T. J. Cullen, and C. N. Ironside, "Picosecond switching induced by saturable absorption in a nonlinear directional coupler," *Appl. Phys. Lett.* **53**, 1144 (1988).
- B. Fluegel, N. Peyghambarian, G. Olbright, M. Lindberg, and S. W. Koch, "Femtosecond studies of coherent transients in semiconductors," *Phys. Rev. Lett.* **59**, 2588 (1987).
- R. L. Fork, O. E. Martinez, and J. P. Gordon, "Negative dispersion using pairs of prisms," *Opt. Lett.* **9**, 150 (1984).
- S. R. Friberg, A. M. Weiner, Y. Silberberg, B. G. Sfez, and P. S. Smith, "Femtosecond switching ion a dual-core-fiber nonlinear coupler," *Opt. Lett.* **13**, 904 (1988).
- D. Fröhlich, A. Nöhte, and K. Reimann, "Observation of the resonant optical Stark effect in a semiconductor," *Phys. Rev. Lett.* **55**, 1335 (1986).
- D. Fröhlich, R. Wille, W. Schlapp, and G. Weimann, "Optical quantum-confined Stark effect in GaAs quantum wells," *Phys. Rev. Lett.* **59**, 1748 (1987).
- D. Grischkowsky, "Self-focusing of light by potassium vapor," *Phys. Rev. Lett.* **24**, 866 (1970).
- D. Grischkowsky, E. Courtens, and J. A. Armstrong, "Observation of self-steepening of optical pulses with possible shock formation," *Phys. Rev. Lett.* **31**, 422 (1973).
- P. A. Harten, S. G. Lee, J. P. Sokoloff, J. R. Salcedo, and N. Peyghambarian, "Noise in a dual dye jet hybridly mode-locked near infrared femtosecond laser," *Opt. Commun.* **99**, xxx (1992).
- H. Haug (Ed.), *"Optical Nonlinearities and Instabilities in Semiconductors"* (Academic Press, San Diego, California, 1988).
- H. Haug and S. W. Koch, *"Quantum Theory of the Optical and Electronic Properties of Semiconductors"* (World Scientific, Singapore, 1990).
- C. Hirlimann, J. F. Morhange, M. A. Kanehisa, A. Chevy, and C. H. Brito-Cruz, "Resonant excitonic optical Stark effect," *Appl. Phys. Lett.* **55**, 2307 (1989).

- R. Jin, C. L. Chuang, H. M. Gibbs, S. W. Koch, J. N. Polky, and G. A. Pubanz, "Picosecond all-optical switching in single-mode GaAs/AlGaAs strip-loaded nonlinear directional couplers," *Appl. Phys. Lett.* **53**, 1791 (1988).
- R. Jin, J. P. Sokoloff, P. A. Harten, C. L. Chuang, S. G. Lee, M. Warren, H. M. Gibbs, N. Peyghambarian, J. N. Polky, and G. A. Pubanz, "Ultrafast modulation with subpicosecond recovery time in a GaAs/AlGaAs nonlinear directional coupler," *Appl. Phys. Lett.* **56**, 993 (1990).
- M. Joffre, D. Hulin, A. Migus, and A. Antonetti, "Dynamics of the optical Stark effect in semiconductors," *J. Mod. Opt.* **35**, 1951 (1988).
- M. Joffre, D. Hulin, J.-P. Foing, J.-P. Chambaret, A. Migus, and A. Antonetti, "Dynamics and Fourier transform studies of the optical Stark effect," *IEEE J. Quant. Electron.* **QE-25**, 2505 (1989).
- T. Juhasz, J. Kuhl, and W. E. Bron, "Dual synchronously pumped and synchronously amplified dye lasers," *Opt. Lett.* **13**, 577 (1988).
- J. D. Kafka and T. Baer, "Prism-pair dispersive delay lines in optical pulse compression," *Opt. Lett.* **12**, 401 (1987).
- M. P. Kesler and E. P. Ippen, "Subpicosecond gain dynamics in GaAlAs laser diodes," *Appl. Phys. Lett.* **51**, 1765 (1987).
- J. Kluge, D. Wiechert, and D. von der Linde, "Fluctuations in synchronously mode-locked dye lasers," *Opt. Commun.* **51**, 271 (1988).
- W. H. Knox, "Generation and kilohertz-rate amplification of femtosecond optical pulses around 800 nm," *J. Opt. Soc. Am. B* **4**, 1771 (1987).
- W. H. Knox, "Femtosecond Optical Pulse Amplification," *IEEE J. Quant. Electron.* **24**, 388 (1988).
- W. H. Knox, D. S. Chemla, D. A. B. Miller, J. B. Stark, and S. Schmitt-Rink, "Femtosecond ac Stark effect in semiconductor quantum wells: extreme low- and high-intensity limits," *Phys. Rev. Lett.* **62**, 1189 (1989).
- S. W. Koch, N. Peyghambarian, and M. Lindberg, "Transient and steady-state optical nonlinearities in semiconductors," *J. Phys. C: Solid State Phys.* **21**, 5229 (1988).
- H. Kogelnik, "The future of photonics," *International Conference on Quantum Electronics Technical Digest Series* **9**, 228 (1992).
- D. Kühlke, U. Herpers, and D. von der Linde, "Characteristics of a Hybridly mode-locked cw dye laser," *Appl. Phys. B* **38**, 233 (1985).

- M. J. LaGasse, K. K. Anderson, H. A. Haus, and J. G. Fujimoto, "Femtosecond all-optical switching in AlGaAs waveguides using a single arm interferometer," *Appl. Phys. Lett.* **54**, 2068 (1989).
- D. L. Lee, *"Electromagnetic Principles of Integrated Optics"* (Wiley, New York, 1986).
- S. G. Lee, P. A. Harten, J. P. Sokoloff, R. Jin, B. Fluegel, K. E. Meissner, C. L. Chuang, R. Binder, S. W. Koch, G. Khitrova, H. M. Gibbs, and N. Peyghambarian, "Femtosecond exciton bleaching recovery in the optical Stark effect of GaAs/Al_xGa_{1-x}As multiple quantum wells and directional couplers," *Phys. Rev. B* **43**, 1719 (1991).
- P. LiKamWa, A. Miller, C. B. Park, J. S. Roberts, and P. N. Robson, "All-optical switching of picosecond pulses in a GaAs quantum well waveguide coupler," *Appl. Phys. Lett.* **57**, 1846 (1990).
- P. LiKamWa, A. Miller, J. S. Roberts, and P. N. Robson, "130 ps recovery of all-optical switching in a GaAs multiquantum well directional coupler," *Appl. Phys. Lett.* **58**, 2055 (1991).
- M. Lindberg and S. W. Koch, "Effective Bloch equations for semiconductors," *Phys. Rev.* **B38**, 3342 (1988).
- D. L. MacFarlane, L. W. Casperson, and A. A. Tovar, "Spectral behavior and pulse train instabilities of a synchronously pumped mode-locked dye laser," *J. Opt. Soc. Am. B* **5**, 1144 (1988).
- D. L. MacFarlane, S. M. Janes, L. W. Casperson, and Shuanghua Jiang, "Timing and detuning studies of a hybridly mode-locked dye laser," *IEEE J. Quant. Electron.* **26**, 718 (1990), and references therein.
- S. L. McCall and E. L. Hahn, "Self-induced transparency by pulsed coherent light," *Phys. Rev. Lett.* **18**, 908 (1967).
- S. L. McCall and E. L. Hahn, "Self-induced transparency," *Phys. Rev.* **183**, 457 (1969).
- A. Mysyrowicz, D. Hulin, A. Antonetti, and A. Migus, "'Dressed Excitons' in a multiple-quantum-well structure: evidence for an optical Stark effect with femtosecond response time," *Phys. Rev. Lett.* **56**, 2748 (1986).
- G. H. C. New and J. M. Catherall, "Perturbations and instabilities in laser mode-locking", in *"Optical Instabilities,"* R. W. Boyd, M. G. Raymer, and L. M. Narducci (Editors), (Cambridge University Press, Cambridge, 1986).
- G. R. Olbright and G. R. Hadley, "Generation of tunable near-infrared amplified femtosecond laser pulses and time-correlated white-light continuum," *J. Opt. Soc. Am. B* **6**, 1363 (1988).
- S. H. Park, J. F. Morhange, A. D. Jeffery, R. A. Morgan, A. Chavez-Pirson, H. M. Gibbs, S. W. Koch, N. Peyghambarian, M. Derstine, A. C. Gossard, J. H. English, and W.

- Wiegman, "Measurements of room-temperature band-gap-resonant optical nonlinearities of GaAs/AlGaAs multiple quantum wells and bulk GaAs," *Appl. Phys. Lett.* **52**, 1201 (1988).
- V. Petrov, W. Rudolph, U. Stamm, and B. Wilhelmi, "Limits of ultrashort pulse generation in cw mode-locked dye lasers," *Phys. Rev. A* **40**, 1474 (1989).
- N. Peyghambarian, H. M. Gibbs, J. L. Jewell, A. Antonetti, A. Migus, D. Hulin, and A. Mysyrowicz, "Blue-shift of the exciton resonance due to exciton-exciton interaction in a multiple-quantum-well structure," *Phys. Rev. Lett.* **53**, 2433 (1984).
- N. Peyghambarian, S. W. Koch, M. Lindberg, B. Fluegel, and M. Joffe, "Dynamic Stark effect of exciton and continuum states in CdS," *Phys. Rev. Lett.* **62**, 1185 (1989), and references therein.
- N. Peyghambarian and S. W. Koch, *"Nonlinear Photonics"* (Springer-Verlag, New York, 1991).
- H. A. Pike and M. Hercher, "Basis for picosecond structure in mode-locked laser pulses," *J. Appl. Phys.* **41**, 4562 (1970).
- W. H. Press, B. P. Flannery, S. A. Teukolsky, and W. T. Vetterling, *"Numerical Recipes"* (Cambridge University Press, Cambridge, 1986).
- J. E. Rothenberg and D. Grischkowsky, "Observation of the formation of an optical intensity shock and wave breaking in the nonlinear propagation of pulses in optical fibers," *Phys. Rev. Lett.* **62**, 531 (1989).
- W. Rudolph and B. Wilhelmi, *"Light Pulse Compression"* (Harwood, London, 1989).
- S. Schmitt-Rink, D. S. Chemla, and D. A. B. Miller, "Theory of transient excitonic optical nonlinearities in semiconductor quantum-well structures," *Phys. Rev. B* **32**, 6601 (1985).
- S. Schmitt-Rink, D. S. Chemla, and D. A. B. Miller, "Linear and nonlinear optical properties of semiconductor quantum wells," *Advances in Physics* **38**, 89 (1989).
- Y. R. Shen and G.-Z. Yang, "Theory of self-phase modulation and spectral broadening" in *"The Supercontinuum Laser Source,"* R. R. Alfano, Ed. (Springer-Verlag, New York, 1989).
- R. E. Slusher and H. M. Gibbs, "Self-induced transparency in atomic rubidium," *Phys. Rev. A* **5**, 1634 (1972).
- K. Smith, W. Sibbett, and J. R. Taylor, "Subpicosecond generation via hybrid mode-locking of Styryl 9 in the near infra-red," *Opt. Commun.* **49**, 359 (1984).
- J. P. Sokoloff, P. A. Harten, R. Jin, C. L. Chuang, M. Warren, H. M. Gibbs, S. G. Lee, and N. Peyghambarian, "Subpicosecond all-optical modulation using the optical Stark effect in a nonlinear directional coupler," *Proc. SPIE* **1138**, 13 (1989).

- Spectra Physics Laser Products Division, "Model 451, 452A, 453, and 454 RF Leakage Reducer and Electronic Modules Service Manual," ch. 4, part number 0000-091A, rev. B, Mountain View (1990).
- D. E. Spence, P. N. Kean, and W. Sibbett, "60-fs pulse generation from a self-mode-locked Ti:sapphire laser," *Opt. Lett.* **16**, 42 (1991).
- M. S. Stix, M. P. Kesler, and E. P. Ippen, "Observation of subpicosecond dynamics in GaAlAs laser diodes," *Appl. Phys. Lett.* **48**, 1722 (1986).
- J. P. van der Ziel and R. A. Logan, "Dispersion of the group velocity refractive index in GaAs double heterostructure lasers," *IEEE J. Quant. Electron.* **QE-19**, 164 (1983).
- D. von der Linde, "Characterization of the noise in continuously operating mode-locked lasers," *Appl. Phys. B* **39**, 201 (1986).
- A. Von Lehmen, D. S. Chemla, J. E. Zucker, and J. P. Heritage, "Optical Stark effect on excitons in GaAs quantum wells," *Opt. Lett.* **11**, 609 (1986).
- K. Watanabe, H. Nakano, A. Honold, and Y. Yamamoto, "Optical nonlinearities of excitonic self-induced transparency solitons: toward ultimate realization of squeezed states and quantum nondemolition measurement," *Phys. Rev. Lett.* **62**, 2257 (1989).
- J. S. Weiner, D. S. Chemla, D. A. B. Miller, H. A. Haus, A. C. Gossard, W. Wiegman, and C. A. Burrus, "Highly anisotropic optical properties of single quantum well waveguides," *Appl. Phys Lett.* **47**, 664 (1985).